Mathematical Modelling and Numerical Analysis Will be set by the publisher
Modélisation Mathématique et Analyse Numérique

MIMETIC FINITE DIFFERENCE APPROXIMATION OF FLOWS IN FRACTURED POROUS MEDIA *

Paola F. Antonietti[1], Luca Formaggia[2], Anna Scotti[3], Marco Verani[4] and Nicola Verzotti[5]

Abstract. We present a possible framework for the numerical simulation of flow in fractured porous media that couples mimetic finite differences for the porous matrix with a finite volume scheme for the flow in the fractures. The resulting method is theoretically analyzed in the case of a single fracture. Moreover, several numerical experiments show the capability of the method to deal also with complicated networks of fractures. Thanks to the implementation of rather general coupling conditions, it encompasses both "conductive fractures", *i.e.*, fractures with high permeability and "sealed fractures", *i.e.*, fractures with low permeability which act as a flow barrier.

1991 Mathematics Subject Classification. 65N30, 35Q86,76S05.

November 5, 2015.

Introduction

The simulation of underground flows is of great interest for a large number of applications, ranging from energy production to water resources management: oil fields exploitation, geothermal energy, nuclear waste and carbon dioxide storage, and groundwater contamination. In all the aforementioned applications, at very different length scales, the heterogeneity of the porous medium has a major impact on the flow. Geological applications are often characterized by the presence of layers of different materials, with permeability that can span several orders of magnitude within the domain of interest. Moreover, tectonic stresses, or sometimes

Keywords and phrases: Mimetic finite differences, flow in fractured porous media

* *Paola F. Antonietti, Anna Scotti and Marco Verani have been partially funded by INdAM - GNCS Project 2015 "Non-standard numerical methds for geophysics". Paola F. Antonietti has been also partially supported by SIR Project n. RBSI14VT0S "PolyPDEs: Non-conforming polyhedral finite element methods for the approximation of partial differential equations" funded by MIUR. The fourth author has been also partially supported by the Italian research grant Prin 2012 2012HBLYE4 "Metodologie innovative nella modellistica differenziale numerica".*

[1] MOX–Laboratory for Modeling and Scientific Computing, Dipartimento di Matematica, Politecnico di Milano, Piazza Leonardo da Vinci 32, 20133 Milano, Italy. paola.antonietti@polimi.it

[2] MOX–Laboratory for Modeling and Scientific Computing, Dipartimento di Matematica, Politecnico di Milano, Piazza Leonardo da Vinci 32, 20133 Milano, Italy. luca.formaggia@polimi.it

[3] MOX–Laboratory for Modeling and Scientific Computing, Dipartimento di Matematica, Politecnico di Milano, Piazza Leonardo da Vinci 32, 20133 Milano, Italy. anna.scotti@polimi.it

[4] MOX– Laboratory for Modeling and Scientific Computing, Dipartimento di Matematica, Politecnico di Milano, Piazza Leonardo da Vinci 32, 20133 Milano, Italy. marco.verani@polimi.it

[5] MOX–Laboratory for Modeling and Scientific Computing, Dipartimento di Matematica, Politecnico di Milano, Piazza Leonardo da Vinci 32, 20133 Milano, Italy. nicola.verzotti@gmail.com

human activities, produce fractures at different space scales, ranging from micro-fractures up to large fractures and faults. While the local effect of small fractures on the permeability of the rock can be accounted for by homogenization, large features should be explicitly included in the model. The contribution of fractures to the overall flow may differ. We may have a sealing effect if a fault is filled with low permeable material, like clay, or high conductivity fractures that induce a preferential direction to the overall flow.

Fractures are characterized by a small aperture compared to their typical length and the size of the domain. For this reason, a common choice in the mathematical modeling of fractures consists in replacing the d-dimensional region occupied by the fracture with a $(d-1)$-dimensional interface. From a computational viewpoint, this avoids the need for an extremely fine grid to resolve the fracture, which is effectively replaced by a discontinuity surface. A suitable reduced $(d-1)$-dimensional problem is then solved on the surfaces representing the fractures, with coupling conditions accounting for the exchange of fluid between the fracture and the porous medium.

In spite of its limitations, Darcy's law [11], possibly in its multiphase generalization, is still the most widespread mathematical model for flows in porous media. If we assume that the fractures are filled by a porous medium with different porosity and permeability than the surrounding porous matrix, Darcy's law can be used also for the $(d-1)$-dimensional flow problem along the fractures. Moreover, this is a valid choice also if we consider hollow fractures with small aperture, thanks to the parallel plates approximation, cf. [1], for example. A reduced model for flow in fractures has been first derived in [3] in the case of very permeable fractures. Later on, in [48] the model has been generalized to treat also the case of fractures with low permeability, *i.e.*, acting as barriers for the flow. Moreover, the case of fractures that are entirely immersed in the domain has been analyzed in [4]. This $(d-1)$-dimensional model has also been extended to the case of two phase flow in [43] and [40]. One of the main issues concerning discretization of the flow in heterogeneous media is the quality of the computational grid. In traditional approaches indeed we usually require geometric conformity, *i.e.*, the fractures should be aligned with the edges of the grid. However, in realistic cases with a large number of fractures this constraint can be difficult to obey, in particular in the case of small intersection angles, or nearly coincident fractures. Geometric conformity can lead either to very fine grids, or to low-quality elements (small angles, high aspect ratios). For most numerical methods a poor quality of the grid reflects on the accuracy of the solution. To overcome this difficulty a possible solution is to perform suitable simplifications of the fracture network, relying on the hypothesis that the actual position and geometry of the fractures are affected by uncertainty [47, 49]. On the other hand, another possible strategy consists in the use of non-conforming discretizations based, for instance, on the eXtended Finite Element Method (XFEM), thus allowing the fractures to arbitrarily cut a fairly regular and coarse grid [34, 40]. If a good quality grid is mandatory for the accuracy and convergence of finite volume and standard finite element methods, this is not true for Mimetic Finite Differences (MFD) as well as for their ultimate evolution into the Virtual Element Methods (VEM) [12], which are well known to be robust even in the presence of polygonal/polyhedral, distorted and highly anisotropic grids. Thanks to their great flexibility and their capability of preserving the fundamental properties of the underlying physical and mathematical models, the use of MFD methods has remarkably increased in the last years, with application to diffusion-type problems [6, 13, 27, 29–32], electromagnetism [26, 28], plate equations [15], non-linear and control problems [5, 7–9], shape optimization [10], and to model two-phase flows [46]. We refer to [14] and [45] for a comprehensive review on MFD schemes. Moreover, very recently VEM and MFD have been employed to model flows in networks of fractures [16, 17] and flows in fractured porous media [2]. We remark that the approach proposed in our work differs from that of [2] where a fully primal formulation is considered and less general coupling conditions, where pressure is assumed to be continuous across the fracture, are used. We also mention a novel approach to the computation of three-dimensional flow in a discrete fracture network which relies on a PDE-constrained optimization algorithm and is able to accomodate different meshing and discretization procedures within each fracture [19–22]. Finally, we recall the general framework of gradient discretizations. A recent presentation of the method for the numerical analysis of diffusion equations is found in [37], yet it has been applied to linear, nonlinear and nonlocal elliptic and parabolic equations [36]. This abstract setting covers at the same time many well known discretisations, as, for example, classical conforming and mixed finite elements,

multi-point flux approximation schemes, hybrid mixed methods and nodal MFD schemes. It has recently been applied also to fractured porous media flow [23, 25]. It deserves with no doubt further investigation also in relation with our work.

The aim of this paper is to study whether the Mimetic Finite Difference method can be succesfully used to simulate flows in fractured porous media. Our physical model is based on the (mixed form of the) Darcy's equations for the porous medium (or bulk) flow coupled with the (primal form of the) Darcy's equations for the fracture flow. The resulting system of equations is then closed imposing suitable physically consistent coupling conditions along the bulk/fracture interfaces. We present the weak formulation of new coupled problem and prove its well-posedness. We remark that our approach is different from the one usually employed in the literature, where either the mixed or the primal form of the Darcy's equations are considered for both bulk and fracture flow. Our choice is motivated by the fact that the coupling conditions at the interfaces between bulk and fracture flow involve only the fracture pressure. Therefore, the fracture velocity is not required in practice and a primal formulation can be employed within the fracture network, without loosing any information. Moreover, this brings some simplification in the analysis and allows the direct use of existing codes for discrete fracture networks, like the one described in [44], that employ the primal formulation of the Darcy's problem. From the numerical viewpoint, we propose to employ MFD methods to discretize the bulk equations and a two-point finite volume scheme for the fracture network. To show the effectiveness of the proposed approach we numerically test it on two-dimensional test cases.

The paper is structured as follows. In Section 1 we introduce the governing equations. The weak formulation of the coupled problem and its well-posedness are addressed in Section 2 in the case of a single fracture that cuts the domain into two disjoint subdomains. The extension of the proposed model to the case of a network of partially immersed fractures is discussed in Section 3. The numerical method is presented in Section 4 where it is also shown that the resulting fully coupled discrete problem admits a unique solution. In Section 5 we present a set of two–dimensional numerical experiments showing the robustness and optimal convergence properties featured by the proposed scheme. Finally, in Section 6 we draw some conclusions.

1. Model problem

This section is devoted to the presentation of the governing equations. Throughout the paper we will adopt the standard notation for Sobolev spaces. More precisely, for $D \subset \mathbb{R}^d$, $d = 2, 3$, and for a real number $s \geq 0$, $H^s(D)$ will denote the standard Sobolev space of order s, endowed with the usual norm $\|\cdot\|_{H^s(D)}$ and seminorm $|\cdot|_{H^s(D)}$. For a $(d-1)$-dimensional manifold $\Gamma \subset D$, we denote by $H^s(\Gamma)$ the usual Sobolev surface space, cf. [38]. For $s = 0$ we will write $L^2(\cdot)$ instead of $H^0(\cdot)$. In the following the symbol $\lesssim$ will signify that the inequality holds up to a multiplicative constant that is independent of the discretization parameter.

To describe an incompressible fluid flow problem in a d-dimensional fractured porous media, $d = 2, 3$, we need the following ingredients: *i)* the governing equations for the porous medium (or bulk) flow; *ii)* the governing equations for the fracture flow; *iii)* suitable physically consistent coupling conditions along the bulk/fractures interfaces; cf. Figure 1 for a sketch of the mathematical model in a three-dimensional configuration ($d = 3$). Let $\Omega \subset \mathbb{R}^d$, $d = 2, 3$, be an open, bounded, convex polygonal/polyhedral domain representing the porous matrix. To keep the presentation as simple as possible, we will assume that there is only one $(d-1)$-dimensional manifold $\Gamma \subset \mathbb{R}^{d-1}$ representing a fracture that cuts Ω into two disjoint subregions, say Ω_1 and Ω_2, and that the measure of Γ is uniformly bounded, *i.e.*, $|\Gamma| \lesssim 1$. We remark that the extension to the case of a finite number of (possibly intersecting) fractures or "partially immersed" fractures can be handled in a similar way but in such a case the mathematical model and the functional setting are much more complex; this will be quickly discussed in Section 3. We assume that the boundary of Ω is decomposed into two non-intersecting subsets, *i.e.*, $\partial\Omega = \Gamma_{\rm D} \cup \Gamma_{\rm N}$, with $\Gamma_{\rm D} \cap \Gamma_{\rm N} = \emptyset$, and $\Gamma_{\rm D} \neq \emptyset$, and set $\Gamma_{{\rm D},i} = \partial\Omega_i \cap \Gamma_{\rm D}$ and $\Gamma_{{\rm N},i} = \partial\Omega_i \cap \Gamma_{\rm N}$ for $i = 1, 2$. Finally, $\mathbf{n}_\Gamma$ denotes the unit normal vector to Γ with a fixed orientation (from Ω_1 to Ω_2) and $\boldsymbol{\tau}_\Gamma$ denotes the $\mathbb{R}^{d\times d-1}$ matrix whose columns form an orthonormal basis for the tangent space at each $x \in \Gamma$.

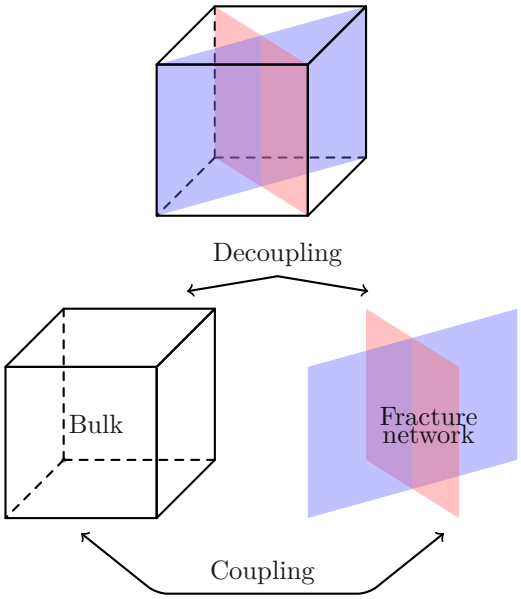

FIGURE 1. Sketch of the mathematical model in a three-dimensional configuration ($d = 3$).

1.1. Governing equations

We first present the governing equations for the bulk flow. To this aim, let $\mathbf{K} \equiv \mathbf{K}(x) \in \mathbb{R}^{d\times d}$ be the bulk permeability tensor, which is assumed to satisfy the following (classical) regularity assumptions:

i) $\mathbf{K}$ is a symmetric tensor whose entries are bounded, piecewise continuous real-valued functions;
ii) there exists $\kappa_\star, \kappa^\star > 0$ such that

$$0 < \kappa_\star \leq \boldsymbol{\zeta}^{\mathrm{T}}\mathbf{K}(x)\boldsymbol{\zeta} \leq \kappa^\star \quad \forall \boldsymbol{\zeta} \in \mathbb{R}^d \setminus \{0\} \quad \text{a.e. } x \in \overline{\Omega}. \tag{1}$$

Given a function $f \in L^2(\Omega)$ representing a source term or a sink and $g_D \in H^{1/2}(\Gamma_{\mathrm{D}})$, we consider the Darcy's law to model the motion of a incompressible fluid in each domain Ω_i, $i = 1, 2$, with pressure p_i and velocity $\mathbf{u}_i$:

$$\begin{cases} \mathbf{K}_i\nabla p_i + \mathbf{u}_i = 0 & \text{in } \Omega_i, \\ \nabla \cdot \mathbf{u}_i = f_i & \text{in } \Omega_i, \\ p_i = g_D & \text{on } \Gamma_{\mathrm{D},i}, \\ \mathbf{u}_i \cdot \mathbf{n} = 0 & \text{on } \Gamma_{\mathrm{N},i}, \end{cases} \tag{2}$$

where $f_i = f|_{\Omega_i}$, $\mathbf{K}_i = \mathbf{K}|_{\Omega_i}$, $i = 1, 2$, and $\mathbf{n}$ denotes the outward unit normal vector to $\partial\Omega$.

The second ingredient is represented by the governing equations for the fracture flow. We consider a reduced model consisting in modeling the fracture as a $(d-1)$–dimensional manifold immersed in an d-dimensional object. Roughly speaking, the reduced model can be obtained writing the Darcy's equations on the fracture in the normal and tangential components and then integrating the tangential component along the thickness $\ell_\Gamma \equiv \ell_\Gamma(x)$ of the fracture domain, which is typically some orders of magnitude smaller than the size of the domain Ω. We refer to [48] for more details. The fracture flow is then characterized by a permeability tensor $\mathbf{K}_\Gamma$, which is assumed

i) to have a block-diagonal structure of the form

$$\mathbf{K}_\Gamma = \begin{bmatrix} \kappa_\Gamma^n & 0 \\ 0 & \kappa_\Gamma^\tau \end{bmatrix},$$

where κ_Γ^τ is a $(d-1)$ positive definite tensor (it reduces to a positive number for $d=2$).

By this we mean that the material contained in the fracture (before the model reduction process has been carried out) has a permeability that can be written in the stated form, and which may vary along the fracture but not across the thickness of the fracture. We will see later on that in the reduced model κ_γ^n and κ_Γ^τ play very different roles and the effective normal and tangential permeability of the fracture scale differently with respect to the fracture thickness;

ii) to satisfy the same condition stated in (1) for the bulk permeability, for $x \in \Gamma$.

We recall that $\mathbf{n}_\Gamma$ denotes the unit normal vector oriented from Ω_1 to Ω_2 so that $\mathbf{n}_\Gamma \equiv \mathbf{n}_1$, $\mathbf{n}_1$ being the unit normal vector that point outward from Ω_1. With the above notation, we define, for a regular enough function v, its *jump* and *average* across Γ as

$$[\![v]\!] = v_1 - v_2, \quad \{v\} = \frac{1}{2}(v_1 + v_2),$$

respectively, where v_i is the restriction of a (regular enough) function v to Ω_i, $i = 1, 2$.

Setting $\partial\Gamma_{\mathrm{N}} = \Gamma \cap \Gamma_{\mathrm{N}}$ and $\partial\Gamma_{\mathrm{D}} = \Gamma \cap \Gamma_{\mathrm{D}}$ (we assume $\partial\Gamma_{\mathrm{D}} \neq \emptyset$), and denoting by p_Γ and $\boldsymbol{q}_\Gamma$ the fracture pressure and flux, respectively, the governing equations for the fracture flow read

$$\begin{cases} \kappa_\Gamma \nabla_\tau p_\Gamma + \boldsymbol{q}_\Gamma = 0 & \text{in } \Gamma, \\ \nabla_\tau \cdot \boldsymbol{q}_\Gamma = \ell_\Gamma f_\Gamma + [\![\boldsymbol{u} \cdot \mathbf{n}_\Gamma]\!] & \text{in } \Gamma, \\ p_\Gamma = g_{\mathrm{D}} & \text{on } \partial\Gamma_{\mathrm{D}}, \\ \boldsymbol{q}_\Gamma \cdot \boldsymbol{\tau}_\Gamma = 0 & \text{on } \partial\Gamma_{\mathrm{N}}, \end{cases} \tag{3}$$

where

$$\kappa_\Gamma = \ell_\Gamma \kappa_\Gamma^\tau, \tag{4}$$

and where we have assumed that both f_Γ and $[\![\boldsymbol{u} \cdot \mathbf{n}_\Gamma]\!]$ belong to $L^2(\Gamma)$. Eliminating the flux variable $\boldsymbol{q}_\Gamma$ we can rewrite (3) in the following primal form

$$\begin{cases} -\nabla_\tau \cdot (\kappa_\Gamma \nabla_\tau p_\Gamma) = \ell_\Gamma f_\Gamma + [\![\mathbf{u} \cdot \mathbf{n}_\Gamma]\!] & \text{in } \Gamma, \\ p_\Gamma = g_{\mathrm{D}} & \text{on } \partial\Gamma_{\mathrm{D}}, \\ -\kappa_\Gamma \nabla_\tau p_\Gamma \cdot \boldsymbol{\tau}_\Gamma = 0 & \text{on } \partial\Gamma_{\mathrm{N}}, \end{cases} \tag{5}$$

which will be used in the following as a starting point to derive the two-point finite volume scheme.

Finally, we provide the interface conditions to couple problems (2) and (3) or, equivalently, problems (2) and (5). Following [48], let $\xi \in [0, 1]$, then the coupling conditions are given by

$$\frac{2\xi - 1}{4} \eta_\Gamma [\![\mathbf{u} \cdot \mathbf{n}_\Gamma]\!] = \{p\} - p_\Gamma \qquad \text{on } \Gamma, \tag{6a}$$

$$\eta_\Gamma \{\mathbf{u} \cdot \mathbf{n}_\Gamma\} = [\![p]\!] \qquad \text{on } \Gamma, \tag{6b}$$

where $\eta_\Gamma = \ell_\Gamma (\kappa_\Gamma^n)^{-1}$. Motivated by the fact that the coupling conditions (6) involve only the pressure in the fracture p_Γ and not the flux $\boldsymbol{q}_\Gamma$, we will focus on the coupled problem (2)–(5), where the primal form of the Darcy's equations is considered in the fracture. This is different from the approaches considered, for example,

in [48], where the mixed form of the Darcy's equations is solved in the fracture. In the next section we then present the weak formulation of problem (2)–(5) supplemented with the coupling conditions (6) and discuss its well posedeness. This will be instrumental to set up the approximation scheme that will be discussed in Section 4.

2. Weak formulation and its well-posedness

We introduce the following spaces

$$
\begin{aligned}
Q &= \{q = (q_1, q_2) \in L^2(\Omega_1) \times L^2(\Omega_2)\},\\
\mathbf{W} &= \{\mathbf{v} = (\mathbf{v}_1, \mathbf{v}_2) \in H(\mathrm{div}, \Omega_1) \times H(\mathrm{div}, \Omega_2) :\ \mathbf{v}_i \cdot \mathbf{n}_\Gamma \in L^2(\Gamma), i = 1, 2\},\\
V_{0,\partial\Gamma_\mathrm{D}} &= \{v \in H^1(\Gamma) :\ v = 0 \text{ on } \partial\Gamma_\mathrm{D}\},
\end{aligned}
$$

with the associated norms

$$
\begin{aligned}
\|q\|_Q^2 &= \sum_{i=1}^{2} \|q_i\|^2_{L^2(\Omega_i)} && \forall q \in Q,\\
\|\mathbf{v}\|^2_{\mathbf{W}} &= \sum_{i=1}^{2} \left(\|\mathbf{v}_i\|^2_{L^2(\Omega)} + \|\nabla \cdot \mathbf{v}_i\|^2_{L^2(\Omega)} + \|\mathbf{v}_i \cdot \mathbf{n}_\Gamma\|^2_{L^2(\Gamma)} \right)^2 && \forall \mathbf{v} \in \mathbf{W},\\
\|v\|^2_{V_{0,\partial\Gamma_\mathrm{D}}} &= \|v\|_{H^1(\Gamma)} && \forall v \in V_{0,\partial\Gamma_\mathrm{D}}.
\end{aligned}
$$

Note that we are requesting more regularity on the velocity $\mathbf{v}$ than mere $H(\mathrm{div}, \Omega_1) \times H(\mathrm{div}, \Omega_2)$. This is required to accommodate the Robin-type interface condition given by (6a), see [48, 50]. It can be shown that the spaces $Q, \mathbf{W}$ and $V_{0,\partial\Gamma_\mathrm{D}}$ are Hilbert spaces with scalar product inducing the above stated norms. For further use, we introduce the space $\mathbf{W}_{0,\Gamma_\mathrm{N}} = \{\mathbf{v} \in \mathbf{W} :\ \mathbf{v}_i \cdot \mathbf{n} = 0 \text{ on } \Gamma_{\mathrm{N},i},\ i = 1, 2\}$.

Next, let the bilinear forms $a_\xi : \mathbf{W}_{0,\Gamma_\mathrm{N}} \times \mathbf{W}_{0,\Gamma_\mathrm{N}} \to \mathbb{R}$, $\mathcal{B} : \mathbf{W}_{0,\Gamma_\mathrm{N}} \times Q \to \mathbb{R}$ and $a_\Gamma : V_{0,\partial\Gamma_\mathrm{D}} \times V_{0,\partial\Gamma_\mathrm{D}} \to \mathbb{R}$ be defined as follows

$$
\begin{aligned}
a_\xi(\mathbf{u}, \mathbf{v}) &= \sum_{i=1}^{2} \int_{\Omega_i} \mathbf{K}_i^{-1} \mathbf{u}_i \cdot \mathbf{v}_i \,\mathrm{dx} + \sum_{i=1}^{2} \int_\Gamma \frac{\eta_\Gamma}{2} \left(\xi \mathbf{u}_i \cdot \mathbf{n}_i - (1 - \xi)\mathbf{u}_{i+1} \cdot \mathbf{n}_{i+1}\right) \mathbf{v}_i \cdot \mathbf{n}_i \,\mathrm{ds},\\
\mathcal{B}(\mathbf{u}, q) &= \sum_{i=1}^{2} \int_{\Omega_i} (\nabla \cdot \mathbf{u}_i) q_i \,\mathrm{dx},\\
a_\Gamma(\phi, \varphi) &= \int_\Gamma \kappa_\Gamma \nabla_\tau \phi \cdot \nabla_\tau \varphi \,\mathrm{ds},
\end{aligned}
$$

where we assume that the index i varies in $\mathbb{Z}/2\mathbb{Z}$, *i.e.*, $2 + 1 = 1$. With the above notation, the weak formulation of problem (2)–(5) complemented with the coupling conditions (6) reads as follows: find $\mathbf{u} = (\mathbf{u}_1, \mathbf{u}_2) \in \mathbf{W}_{0,\Gamma_\mathrm{N}}$,

$p = (p_1, p_2) \in Q$, and $p_\Gamma \in V_{0,\partial\Gamma_\mathrm{D}}$ such that

$$a_\xi(\mathbf{u}, \mathbf{v}) - \mathcal{B}(\mathbf{v}, p) + \int_\Gamma [\![\mathbf{v} \cdot \mathbf{n}_\Gamma]\!] p_\Gamma \,\mathrm{ds} = \sum_{i=1}^{2} \int_{\Gamma_{\mathrm{D},i}} g_\mathrm{D} \mathbf{v}_i \cdot \mathbf{n} \,\mathrm{ds}, \tag{7a}$$

$$\mathcal{B}(\mathbf{u}, q) = \sum_{i=1}^{2} \int_{\Omega_i} f_i q_i \,\mathrm{dx}, \tag{7b}$$

$$a_\Gamma(p_\Gamma, \varphi) - \int_\Gamma [\![\mathbf{u} \cdot \mathbf{n}_\Gamma]\!] \varphi \,\mathrm{ds} = \int_\Gamma \ell_\Gamma f_\Gamma \varphi \,\mathrm{ds}, \tag{7c}$$

for all $\mathbf{v} = (\mathbf{v}_1, \mathbf{v}_2) \in \mathbf{W}_{0,\Gamma_\mathrm{N}}$, $q = (q_1, q_2) \in Q$, and $\varphi \in V_{0,\partial\Gamma_\mathrm{D}}$.

Next, we show that formulation (7) is well-posed. We first note that for any $\psi \in L^2(\Gamma)$ the solution $q_\Gamma \in V_{0,\partial\Gamma_\mathrm{D}}$ of

$$a_\Gamma(q_\Gamma, \varphi) = \int_\Gamma \psi\varphi \,\mathrm{ds} + \int_\Gamma \ell_\Gamma f_\Gamma \varphi \,\mathrm{ds} \quad \forall \varphi \in V_{0,\partial\Gamma_\mathrm{D}}, \tag{8}$$

is unique and may be decomposed uniquely as $q_\Gamma = q_\Gamma^0 + q_\Gamma^1(\psi)$, where q_Γ^0 and $q_\Gamma^1(\psi)$ are solutions of

$$a_\Gamma(q_\Gamma^0, \varphi) = \int_\Gamma \ell_\Gamma f_\Gamma \,\mathrm{ds} \qquad \forall \varphi \in V_{0,\partial\Gamma_\mathrm{D}}, \tag{9a}$$

$$a_\Gamma(q_\Gamma^1(\psi), \varphi) = \int_\Gamma \psi\varphi \,\mathrm{ds} \qquad \forall \varphi \in V_{0,\partial\Gamma_\mathrm{D}}, \tag{9b}$$

respectively. Furthermore, we have

$$\|q_\Gamma^0\|_{H^1(\Gamma)} \lesssim \|\ell_\Gamma f_\Gamma\|_{L^2(\Gamma)}, \tag{10a}$$

$$\|q_\Gamma^1(\psi)\|_{H^1(\Gamma)} \lesssim \|\psi\|_{L^2(\Gamma)}, \tag{10b}$$

where the hidden constants depend on $\ell_\Gamma \kappa_*$. It may be recognized that the mapping from $L^2(\Gamma)$ to $H^1(\Gamma)$ defined as $\psi \to q_\Gamma^1(\psi)$ is linear and continuous. Consequently, we can introduce $\mathcal{A}_\xi(\cdot,\cdot) : \mathbf{W} \times \mathbf{W} \to \mathbb{R}$ defined as follows

$$\mathcal{A}_\xi(\mathbf{u}, \mathbf{v}) = a_\xi(\mathbf{u}, \mathbf{v}) + \int_\Gamma q_\Gamma^1([\![\mathbf{u} \cdot \mathbf{n}_\Gamma]\!])[\![\mathbf{v} \cdot \mathbf{n}_\Gamma]\!] \,\mathrm{ds},$$

and rewrite (7a)-(7b) as: find $\mathbf{u} = (\mathbf{u}_1, \mathbf{u}_2) \in \mathbf{W}_{0,\Gamma_\mathrm{N}}$ and $p = (p_1, p_2) \in Q$ such that

$$\mathcal{A}_\xi(\mathbf{u}, \mathbf{v}) - \mathcal{B}(\mathbf{v}, p) = \mathcal{F}_\xi(\mathbf{v}) \qquad \forall \mathbf{v} = (\mathbf{v}_1, \mathbf{v}_2) \in \mathbf{W}_{0,\Gamma_\mathrm{N}}, \tag{11a}$$

$$\mathcal{B}(\mathbf{u}, q) = \mathcal{G}(q) \qquad \forall q = (q_1, q_2) \in Q, \tag{11b}$$

where we have set

$$\mathcal{F}_\xi(\mathbf{v}) = \int_{\Gamma_\mathrm{D}} g_\mathrm{D} [\![\mathbf{v} \cdot \mathbf{n}_\Gamma]\!] \,\mathrm{ds} - \int_\Gamma q_\Gamma^0 [\![\mathbf{v} \cdot \mathbf{n}_\Gamma]\!] \,\mathrm{ds},$$

$$\mathcal{G}(q) = \int_\Omega f q \,\mathrm{dx},$$

and we have used a shorthand notation for the integrals in the right hand sides.

Proposition 2.1. *The form $\mathcal{A}_\xi(\cdot,\cdot) : \mathbf{W} \times \mathbf{W} \to \mathbb{R}$ is bilinear and continuous on $\mathbf{W}$. Moreover, it is coercive on*

$$\widetilde{\mathbf{W}} = \{\mathbf{v} \in \mathbf{W}_{0,\Gamma_N} : \ \mathcal{B}(\mathbf{u}, q) = 0 \quad \forall q \in Q\},$$

provided that $\xi \in (1/2, 1]$.

Proof. Bilinearity of $\mathcal{A}_\xi(\cdot,\cdot)$ is straightforward, as it is sufficient to note that the map $q_\Gamma^1(\cdot)$ is linear by construction. Continuity is a consequence of the fact that the following inequalities hold

$$\left|\sum_{i=1}^{2} \int_{\Omega_i} \mathbf{K}_i^{-1}\mathbf{u}_i \cdot \mathbf{v}_i \,\mathrm{dx}\right| \lesssim \|\mathbf{u}\|_{\mathbf{W}}\|\mathbf{v}\|_{\mathbf{W}},$$
$$\left|\int_\Gamma [\![\mathbf{v}\cdot\mathbf{n}_\Gamma]\!] q_\Gamma^1([\![\mathbf{u}\cdot\mathbf{n}_\Gamma]\!])\,\mathrm{ds}\right| \lesssim \|[\![\mathbf{v}\cdot\mathbf{n}_\Gamma]\!]\|_{L^2(\Gamma)}\|[\![\mathbf{u}\cdot\mathbf{n}_\Gamma]\!]\|_{L^2(\Gamma)},$$

for any $\mathbf{u}, \mathbf{v} \in \mathbf{W}$, where the hidden constant in the first bound depends on κ_*. In order to prove coercivity, we first note that for $\mathbf{v} \in \widetilde{\mathbf{W}}$ we have that $\nabla \cdot \mathbf{v}_i = 0$ in $L^2(\Omega_i)$, $i = 1, 2$, thus yielding $\|\mathbf{v}\|_{\mathbf{W}}^2 = \sum_{i=1}^2 \|\mathbf{v}_i\|_{L^2(\Omega)}^2 + \|\mathbf{v}_i \cdot \mathbf{n}_\Gamma\|_{L^2(\Gamma)}^2$. Now,

$$\sum_{i=1}^{2} \int_{\Omega_i} \mathbf{K}_i^{-1}\mathbf{u}_i \cdot \mathbf{u}_i \,\mathrm{dx} \geq \frac{1}{\kappa^*}\|\mathbf{u}\|_{L^2(\Omega)}^2, \tag{12}$$

$$\int_\Gamma [\![\mathbf{u}\cdot\mathbf{n}_\Gamma]\!] q_\Gamma^1([\![\mathbf{u}\cdot\mathbf{n}_\Gamma]\!])\,\mathrm{ds} = \int_\Gamma \kappa_\Gamma |\nabla_\tau q_\Gamma^1|^2 \,\mathrm{ds} \geq 0. \tag{13}$$

Finally, we note that

$$\sum_{i=1}^{2} \int_\Gamma \frac{\eta_\Gamma}{2} \left(\xi \mathbf{u}_i \cdot \mathbf{n}_i - (1-\xi)\mathbf{u}_{i+1} \cdot \mathbf{n}_{i+1}\right) \mathbf{v}_i \cdot \mathbf{n}_i \,\mathrm{ds} = \int_\Gamma \frac{\eta_\Gamma}{2} \left\{\mathbf{u}\cdot\mathbf{n}_\Gamma\right\}\left\{\mathbf{v}\cdot\mathbf{n}_\Gamma\right\} \,\mathrm{ds} + \xi_0 \int_\Gamma \frac{\eta_\Gamma}{2} [\![\mathbf{u}\cdot\mathbf{n}_\Gamma]\!][\![\mathbf{v}\cdot\mathbf{n}_\Gamma]\!] \,\mathrm{ds},$$

where $\xi_0 = \frac{2\xi-1}{2}$. Let $\widetilde{\ell}_\Gamma = \min_{x\in\Gamma} \ell_\Gamma(x)$, then since $\eta_\Gamma > \frac{\widetilde{\ell}_\Gamma}{\kappa^*}$, we have

$$\begin{aligned}\int_\Gamma \eta_\Gamma \left(\left\{\mathbf{u}\cdot\mathbf{n}_\Gamma\right\}^2 + \xi_0 [\![\mathbf{u}\cdot\mathbf{n}_\Gamma]\!]^2\right) \,\mathrm{ds} \geq & \frac{\widetilde{\ell}_\Gamma}{\kappa^*} \min(1,\xi_0) \int_\Gamma \left(\left\{\mathbf{u}\cdot\mathbf{n}_\Gamma\right\}^2 + [\![\mathbf{u}\cdot\mathbf{n}_\Gamma]\!]^2\right) \,\mathrm{ds} \\ \geq & \frac{\widetilde{\ell}_\Gamma}{\kappa^*} \min(1,\xi_0) \sum_{i=1}^{2} \|\mathbf{u}_i \cdot \mathbf{n}_\Gamma\|_{L^2(\Gamma)}^2.\end{aligned} \tag{14}$$

By collecting the results in (12), (13) and (14) we obtain

$$\mathcal{A}_\xi(\mathbf{u},\mathbf{u}) \geq \frac{\widetilde{\ell}_\Gamma}{\kappa^*} \min(1,\xi_0)\|\mathbf{u}\|_{\mathbf{W}}^2.$$

Therefore, the bilinear form $\mathcal{A}_\xi(\cdot,\cdot)$ is coercive provided $\xi_0 = \frac{2\xi-1}{2} > 0$, *i.e.*, $\xi > 1/2$. □

We remark that the condition $\xi > 1/2$ has been found also by [48].

Proposition 2.2. *The bilinear form $\mathcal{B} : \mathbf{W}_{0,\Gamma_N} \times Q \to \mathbb{R}$ satisfies the inf-sup condition,* i.e.*, there exists $C_\mathcal{B} > 0$ such that*

$$\inf_{q\in Q} \sup_{\mathbf{w}\in\mathbf{W}} \frac{\mathcal{B}(\mathbf{w}, q)}{\|q\|_Q \|\mathbf{w}\|_{\mathbf{W}}} > C_\mathcal{B}.$$

Proof. The result is rather standard and follows the lines of the one given in [48]. For the sake of clarity we report a sketch of the proof in the case of Dirichlet boundary conditions, namely, $\Gamma_N = \emptyset$. For any $q = (q_1, q_2) \in Q$, under the assumption of a sufficiently regular domain Ω, we can find $z \in H^2(\Omega) \cap H_0^1(\Omega)$ solution of

$$\begin{cases} -\triangle z = q & \text{in } \Omega, \\ z = 0 & \text{on } \partial\Omega, \end{cases}$$

satisfying the stability estimate $\|z\|_{H^2(\Omega)} \lesssim \|q\|_{L^2(\Omega)}$. Then, we define the velocities $\mathbf{w}_i$ as the restrictions on Ω_i of $-\nabla z$, *i.e.*,

$$\mathbf{w}_i = (-\nabla z)|_{\Omega_i}, \quad i = 1, 2.$$

Clearly, $\nabla \cdot \mathbf{w}_i = q|_{\Omega_i} \in L^2(\Omega_i)$, $i = 1, 2$ and $[\![\mathbf{w} \cdot \mathbf{n}_\Gamma]\!] = 0$. Moreover, it is straightforward to see that, $\mathcal{B}(\mathbf{w}, q) = \|q\|_Q^2$ and

$$\begin{aligned} \|\mathbf{w}\|_{\mathbf{W}}^2 &= \|\nabla z\|_{L^2(\Omega)}^2 + \|q\|_{L^2(\Omega)}^2 + \sum_{i=1}^{2} \|\mathbf{w}_i \cdot \mathbf{n}_\Gamma\|_{L^2(\Gamma)}^2 \\ &\lesssim \|q\|_{L^2(\Omega)}^2 + \sum_{i=1}^{2} \|\mathbf{w}_i \cdot \mathbf{n}_\Gamma\|_{L^2(\Gamma)}^2, \end{aligned}$$

where the last bound follows from the elliptic regularity estimate $\|\nabla z\|_{L^2(\Omega)} \lesssim \|q\|_{L^2(\Omega)}$. The proof is concluded by observing that,

$$\sum_{i=1}^{2} \|\mathbf{w}_i \cdot \mathbf{n}_\Gamma\|_{L^2(\Gamma)}^2 \lesssim \|q\|_{L^2(\Omega)}^2,$$

thanks to the trace inequality, where the hidden constant depends on $|\Gamma|^{1/2}|\Omega|^{-1/2}$, which is uniformly bounded since $|\Gamma| \lesssim 1$. □

Before proving that problems (7) and (11) are well-posed, we preliminarily show the following equivalence result.

Proposition 2.3. *Problems* (7) *and* (11) *are equivalent.*

Proof. We only show that if $(\mathbf{u}, p) \in \mathbf{W}_{0,\Gamma_N} \times Q$ is a solution of (11) then $(\mathbf{u}, p, p_\Gamma) \in \mathbf{W}_{0,\Gamma_N} \times Q \times V_{0,\partial\Gamma_D}$ is a solution of (7) where

$$p_\Gamma([\![\mathbf{u} \cdot \mathbf{n}_\Gamma]\!]) = q_\Gamma^0 + q_\Gamma^1([\![\mathbf{u} \cdot \mathbf{n}_\Gamma]\!]). \tag{15}$$

The converse is straightforward, so we omit the proof. We first observe that given $\mathbf{u} \in \mathbf{W}_{0,\Gamma_N}$, problems (7c) and (9) are equivalent by construction, *i.e.*, $p_\Gamma = q_\Gamma^0 + q_\Gamma^1([\![\mathbf{u} \cdot \mathbf{n}_\Gamma]\!])$, where p_Γ solves (7c) and q_Γ^0, q_Γ^1 are given by (9). Next, we show that if $(\mathbf{u}, p)$ is a solution of (11) then $(\mathbf{u}, p, p_\Gamma)$ is a solution of (7) where p_Γ is defined as in (15). To this aim, we take the residual of (7a)–(7c) for $\mathbf{u} \in \mathbf{W}_{0,\Gamma_N}$ solution of (11) and $p_\Gamma = q_\Gamma^0 + q_\Gamma^1([\![\mathbf{u} \cdot \mathbf{n}_\Gamma]\!])$, and observe that it is zero since it is identical to the residual of (11). Next, we show that (7) has a unique solution. To this aim assume, by absurd, that $(\mathbf{u}^*, p^*, p_\Gamma^*)$ is a solution of (7a)-(7c) different from $(\mathbf{u}, p, p_\Gamma = q_\Gamma^0 + q_\Gamma^1([\![\mathbf{u} \cdot \mathbf{n}_\Gamma]\!]))$ where $(\mathbf{u}, p)$ is the solution of (11) for the same data. Clearly,

$$p_\Gamma^* = q_\Gamma^0 + q_\Gamma^1([\![\mathbf{u}^* \cdot \mathbf{n}_\Gamma]\!]). \tag{16}$$

Now, from (7b), we have

$$\mathcal{B}(\mathbf{u} - \mathbf{u}^*, q) = 0 \quad \forall q \in L^2(\Omega).$$

Taking $q = \nabla \cdot (\mathbf{u}^* - \mathbf{u})$ and using the definition of the bilinear form $\mathcal{B}(\cdot, \cdot)$ we obtain

$$0 = \mathcal{B}(\mathbf{u} - \mathbf{u}^*, \nabla \cdot (\mathbf{u} - \mathbf{u}^*)) = \|\nabla \cdot (\mathbf{u} - \mathbf{u}^*)\|_{L^2(\Omega)}^2,$$

that is $\nabla\cdot(\mathbf{u}-\mathbf{u}^*)=0$ in $L^2(\Omega)$. Notice that this, in particular, implies $[\![(\mathbf{u}-\mathbf{u}^*)\cdot\mathbf{n}_\Gamma]\!]=0$. Using this identity in (16) we obtain $p^*_\Gamma=p_\Gamma$. Notice that the identity $p^*_\Gamma=p_\Gamma$ could have also been proved by using (7c). Indeed, from (7c) and and using that $[\![(\mathbf{u}-\mathbf{u}^*)\cdot\mathbf{n}_\Gamma]\!]=0$ we have

$$a_\Gamma(p_\Gamma-p^*_\Gamma,\varphi)=0\quad\forall\varphi\in V_{0,\partial\Gamma_{\rm D}},$$

which implies, taking $\varphi=p_\Gamma-p^*_\Gamma$, that $p_\Gamma=p^*_\Gamma$ in $V_{0,\partial\Gamma_{\rm D}}$. Next, using the previous results and subtracting (7a) and (11a) we obtain

$$a_\xi(\mathbf{u}-\mathbf{u}^*,\mathbf{v})=0\quad\forall\mathbf{v}\in\mathbf{W}_{0,\Gamma_{\rm N}}.$$

Taking $\mathbf{v}=\mathbf{u}-\mathbf{u}^*$, we obtain $\mathbf{u}=\mathbf{u}^*$ in $\mathbf{W}_{0,\Gamma_{\rm N}}$. Finally, we are only left to show that $p=p^*$. We employ (7a) and write it for $(\mathbf{u},p,p_\Gamma)$ and $(\mathbf{u}^*,p^*,p^*_\Gamma)$. Subtracting the two equations term by term we obtain

$$a_\xi(\mathbf{u}-\mathbf{u}^*,\mathbf{v})-\mathcal{B}(\mathbf{v},p-p^*)+\int_\Gamma[\![\mathbf{u}\cdot\mathbf{n}_\Gamma]\!]p_\Gamma\,\mathrm{ds}-\int_\Gamma[\![\mathbf{u}^*\cdot\mathbf{n}_\Gamma]\!]p^*_\Gamma\,\mathrm{ds}=0\quad\forall\mathbf{v}\in\mathbf{W}_{0,\Gamma_{\rm N}}.$$

Since $\mathbf{u}=\mathbf{u}^*$ and $p_\Gamma=p^*_\Gamma$,

$$\mathcal{B}(\mathbf{v},p-p^*)=0\quad\forall\mathbf{v}\in\mathbf{W}_{0,\Gamma_{\rm N}}.$$

From the inf-sup condition proved in Proposition 2.2 we obtain $p=p^*$, and the proof is complete. □

Proposition 2.4. *Problems* (7) *and* (11) *are well posed.*

Proof. The proof of the well-posedness of problem (11) is an immediate consequence of Propositions 2.1 and 2.2 and the continuity of the functionals on the right hand side of (11a) and (11b), this latter being guaranteed by the regularity of the boundary datum g_D, the forcing term f and of q^0_Γ. The well-posedness of problem (7) follows from the equivalence of problems (11) and (7), cf. Proposition 2.3. □

3. The case of immersed fracture networks

We now consider the case of a two-dimensional network of immersed fractures, *i.e.*, networks of fractures whose endpoints may not intersect the domain boundary. We refer to the case where at least one endpoint is on the boundary as partially immersed network. A thorough analysis of this case is still ongoing work, some preliminary results may however be found in the literature. For instance, in [4] the case of a single immersed fracture is analyzed, but eventually using a primal formulation only for the pressure. In [24] the authors consider the case of a partially immersed network, yet employing different (simpler) coupling conditions, and a gradient discretization method is proposed for the numerical solution. In this work we limit ourselves to describing the mathematical model and showing, by numerical experiments, that the corresponding discretization by a mimetic/finite volume scheme gives satisfactory results.

A possible situation is the one depicted in Figure 2. In this section Γ indicates the network, which is composed by a set of M_Γ fractures, *i.e.*, $\Gamma=\cup_{k=1}^{M_\Gamma}\overline{\gamma}_k$, each γ_k being (in the 2D case that we consider here) an open segment in $\mathbb{R}^2$. We further assume that, for $j\neq k$

$$\overline{\gamma}_k\cap\overline{\gamma}_j=\partial\gamma_k\cap\partial\gamma_j=i_{kj},\tag{17}$$

that is, the fractures may join only at their end points. Here i_{kj} indicates the intersection point between fracture γ_k and γ_j, which may be empty if the corresponding fractures do not intersect each other. A fracture may reach the boundary, we assume that the angle formed by any couple of intersecting fracture as well as the angle between fractures and domain boundary is bounded from below by a positive angle. As a consequence, the number of fractures intersecting at an intersection point is bounded. We further indicate with $\mathcal{I}=\cup i_{kj}$ the set of all intersection points, while we set $\partial\gamma_k^D=\partial\gamma_k\cap\Gamma_D$, $\partial\gamma_k^N=\partial\gamma_k\cap\Gamma_N$, $\partial\gamma_k^I=\partial\gamma_k\cap\mathcal{I}$ and $\partial\gamma_k^F=\partial\gamma_k\setminus(\partial\gamma_k^D\cup_{s=D,N,I}\partial\gamma_k^s)$, the latter set collecting the "free" fracture endpoints that are strictly contained in Ω. It is understood that some of those sets may be empty, while their union is the whole $\partial\gamma_k$. For $s=D,N,F$

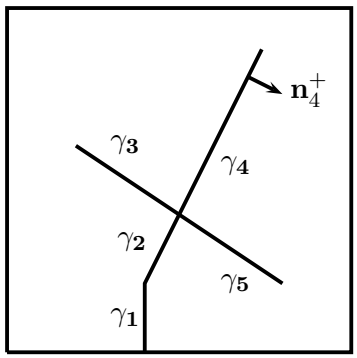

FIGURE 2. Fracture network: a two dimensional example.

we define $\mathcal{I}^s = \cup \partial\gamma_k^s$, and for a given intersection point $i \in \mathcal{I}$ we indicate with $\mathcal{S}_i$ the set of fractures γ_k intersecting in i, *i.e.*, the fractures γ_k such that $\partial\gamma_k^I \cap i \neq \emptyset$.

On each fracture γ_k we can identify two sides, indicated by γ_k^+ and γ_k^-, respectively, and the two associated normals $\mathbf{n}_k^+$ and $\mathbf{n}_k^- = -\mathbf{n}_k^+$. We also associate to each fracture a unique normal by taking $\mathbf{n}_k = \mathbf{n}_k^+$. To simplify notation we indicate by $\mathbf{n}_\Gamma^\pm$ the normal vectors to the network Γ, *i.e.*, $\mathbf{n}_\Gamma^\pm(\mathbf{x}) = \mathbf{n}_k^\pm(\mathbf{x})$ if $\mathbf{x} \in \gamma_k$. Analogously for $\mathbf{n}_\Gamma$. For a function f in $\Omega \setminus \Gamma$ we indicate with $f^\pm$ its traces on $\Gamma^\pm = \cup\gamma_k^\pm$, respectively. This allows to extend the jump and average operators on the network Γ, *i.e.*, $\{f\} = \frac{1}{2}(f^+ + f^-)$ and $[\![f]\!] = f^+ - f^-$. We also extend the previous definitions of $\mathbf{K}_\Gamma$, κ_Γ^n and κ_Γ^τ to the network Γ in a natural way. Finally, in the following we indicate with $\boldsymbol{\tau}_k$ the unit tangent of γ_k at its end points, pointing outwards w.r.t. γ_k. Now, we are ready to formally extend (2) into

$$\begin{cases} \mathbf{K}\nabla p + \mathbf{u} = 0 & \text{in } \Omega \setminus \Gamma, \\ \nabla \cdot \mathbf{u} = f & \text{in } \Omega \setminus \Gamma, \\ p = g & \text{on } \Gamma_{\mathrm{D}}, \\ \mathbf{u} \cdot \mathbf{n} = 0 & \text{on } \Gamma_{\mathrm{N}}\ . \end{cases} \tag{18}$$

As for (5) it is rewritten by imposing continuity of flux and pressure at the intersection points, namely

$$\begin{cases} -\nabla_\tau \cdot (\kappa_\Gamma \nabla_\tau p_\Gamma) = \ell_\Gamma f_\Gamma + [\![\mathbf{u} \cdot \mathbf{n}_\Gamma]\!] & \text{in } \Gamma, \\ p_\Gamma = g_{\mathrm{D}} & \text{on } \mathcal{I}^D, \\ -\kappa_\Gamma \nabla_\tau p_\Gamma \cdot \boldsymbol{\tau}_\Gamma = 0 & \text{on } \mathcal{I}^N \cup \mathcal{I}^F, \\ p_\Gamma = p_i & \text{on } i, \quad \forall i \in \mathcal{I}, \\ \displaystyle\sum_{\gamma_k \in \#i} \kappa_{\gamma_k} \nabla_\tau p_{\gamma_k} \cdot \boldsymbol{\tau}_{\gamma_k} = 0 & \text{on } i, \quad \forall i \in \mathcal{I}. \end{cases}$$

Here, equations on Γ are in fact on each γ_k. Furthermore, we have imposed a zero flux condition on the fracture endpoints $\mathcal{I}^F$, which are immersed in the matrix domain. As for the interface conditions (6), they may be formally rewritten in the same way, where it is understood that they should be applied on each γ_k.

As already pointed out, it is beyond the scope of this paper to give more details on this more complex, yet more realistic, model. We only add that is it possible to formally derive a weak form having the same structure as (7a)-(7c) and to extend to it the numerical discretization techniques presented in the next section for the simplified situation of a single fracture. Indeed, in the section on numerical result we will show an example that considers a network of fractures.

4. Numerical discretization

In this section we present a Mimetic/Finite Volume discretization of the fully coupled problem (7). As a first step, we introduce the mimetic discretization of (7a)-(7b), under the assumption that p_Γ is given (see Section 4.1). Then, we discuss the finite volume discretization of (7c) under the assumption that the velocity field $\mathbf{u}$ is known (see Section 4.2). Finally, in Section 4.3 we present the Mimetic/Finite volume discretization of the fully coupled problem. To keep the presentation as simple as possible, in this section we consider a two-dimensional case, *i.e.*, $d = 2$.

4.1. Mimetic discretization of the bulk problem

In this section we present the mimetic discretization of (7a)-(7b) under the assumption that p_Γ is given. We first introduce some useful notation. Let $\mathcal{T}_h$ be a partition of Ω into non-overlapping (possibly non-convex) polygons E, which are aligned with the fracture Γ. This induces a natural partition of $\mathcal{T}_h$ into two disjoint sets of polygons $\mathcal{T}_{h,1}$ and $\mathcal{T}_{h,2}$ such that $\mathcal{T}_h = \mathcal{T}_{h,1} \cup \mathcal{T}_{h,2}$. In practice, $\mathcal{T}_h$ can be simply built as follows: first Ω is meshed with a Cartesian grid, then the elements across Γ are simply cut in such a way that the resulting polygonal elements are conforming with Γ. This procedure induces also a subdivision of Γ which we call Γ_h. The set of all edges of the decomposition $\mathcal{T}_h$ is denoted by $\mathcal{E}_h$. In order to deal with the coupling conditions (6), and also in view of the discretization of the equation in the fracture, detailed in the next Section 4.2, we number the edges $\hat{\mathsf{e}}_i \in \Gamma_h$ for $i = 1, \dots, N_\Gamma$ and for each $\hat{\mathsf{e}}_i$ we create two edges e_1^i and e_2^i, geometrical identical to $\hat{\mathsf{e}}_i$, which will be associated to $\mathcal{T}_{h,1}$ and $\mathcal{T}_{h,2}$, respectively, so that each subset $\mathcal{T}_{h,i}$ is complemented with its own fracture edges. In other words, any original fracture edge $\hat{\mathsf{e}}_i$ created by the mesh generation procedure described above is replaced, for the bulk problem, by two edges, e_1^i and e_2^i. In view of this discussion, the set $\mathcal{E}_h$ can be decomposed as follows

$$\mathcal{E}_h = \cup_{i=1}^2 \left(\mathcal{E}_{h,i}^0 \cup \mathcal{E}_{h,i}^\Gamma \cup \mathcal{E}_h^{\Gamma_{\mathrm{D},i}} \cup \mathcal{E}_h^{\Gamma_{\mathrm{N},i}} \right), \tag{19}$$

where $\mathcal{E}_{h,i}^0$ is the set of internal edges of $\mathcal{T}_{h,i}$, $\mathcal{E}_{h,i}^\Gamma$ contains the (duplicated) edges of $\mathcal{T}_{h,i}$ belonging to the fracture Γ, while $\mathcal{E}_h^{\Gamma_{\mathrm{D},i}}$ is the set of edges belonging to $\Gamma_{\mathrm{D},i}$ and $\mathcal{E}_h^{\Gamma_{\mathrm{N},i}}$ is the set of edges belonging to $\Gamma_{\mathrm{N},i}$. The sets of vertexes of $\mathcal{T}_h$ is denoted by $\mathcal{V}_h$. The sets of vertexes and edges of a particular element E are denoted by $\mathcal{V}_h^E$ and $\mathcal{E}_h^E$, respectively. For any edge $\mathsf{e} \subset \partial E$ of every polygon $E \in \mathcal{T}_h$, we define a unit normal vector $\mathbf{n}_E^\mathsf{e}$ that points outside of E. Finally, for each element $E \in \mathcal{T}_h$, let h_E be its diameter, and we set $h = \max_{E \in \mathcal{T}_h} h_E$. Following [29] we require that the decomposition $\mathcal{T}_h$ satisfies the following shape regularity assumptions:

- **A1:** The number of edges of any element E is uniformly bounded;
- **A2:** There exists $\tau > 0$ such that every element E is star-shaped with respect to every point of a ball centered at a point $C_E \in E$ and with radius τh_E;
- **A3:** For any element E and for any edge $\mathsf{e} \subset \partial E$ it holds $|\mathsf{e}| \gtrsim h_E$, where $|\mathsf{e}|$ denotes the length of e.

Now let us introduce the mimetic spaces. We denote by Q^h the discrete space representing the degrees of freedom of the scalar variables. More precisely, we associate the degrees of freedom of the scalar variable to mesh cells so that for $\boldsymbol{q}_h \in Q^h$ we have $\boldsymbol{q}_h = \{q_E\}_{E \in \mathcal{T}_h}$, being $q_E \in \mathbb{R}$ the value of the discrete pressure associated to the element E. By definition, the dimension of Q^h is equal to the number of elements in $\mathcal{T}_h$. Let us now introduce the space $\mathbf{W}^h$ of discrete velocities. To every element $E \in \mathcal{T}_h$ and to every edge $\mathsf{e} \subseteq \partial E$ we associate a flux degree of freedom G_E^e. For each interior edge $\mathsf{e} \in \mathcal{E}_h^0 \setminus (\mathcal{E}_{h,1}^\Gamma \cup \mathcal{E}_{h,2}^\Gamma)$ not belonging to the fracture Γ and shared by two polygons E^+ and E^- we enforce flux continuity, *i.e.*, $G_{E^+}^\mathsf{e} = G_{E^-}^\mathsf{e}$. On the other hand, in view of the coupling conditions (6), we do not require any flux continuity across the fracture. Thus, for $\mathbf{G} \in \mathbf{W}^h$, we have $\mathbf{G} = \{G^\mathsf{e}\}_{\mathsf{e} \in \mathcal{E}_h}$, with $G^\mathsf{e} \in \mathbb{R}$, and the dimension of $\mathbf{W}^h$ is equal to the cardinality of $\mathcal{E}_h$ (see equation (19)). The discrete subspace $\mathbf{W}_{0,\Gamma_\mathrm{N}}^h \subseteq \mathbf{W}^h$ is defined by incorporating the homogeneous Neumann boundary conditions on Γ_N, *i.e.*,

$$\mathbf{W}_{0,\Gamma_\mathrm{N}}^h = \{\mathbf{G} \in \mathbf{W}^h : \ \mathbf{G}^\mathsf{e} = 0 \quad \forall \mathsf{e} \in \mathcal{E}_h^{\Gamma_{\mathrm{N},i}} \ i = 1, 2\} \subseteq \mathbf{W}^h.$$

For further use we introduce the jump operator across each fracture edge, *i.e.*,

$$[\![\mathbf{G}]\!]_{\hat{\mathsf{e}}_i} = G^{\mathsf{e}_1^i} - G^{\mathsf{e}_2^i}, \quad i = 1, \dots, N_\Gamma. \tag{20}$$

We also introduce two projection operators, denoted by the superscript I, from $L^1(\Omega)$ and $H(\mathrm{div}, \Omega)$ onto Q^h and $\mathbf{W}^h$, respectively, as follows

$$\begin{aligned} \boldsymbol{q}^{\mathrm{I}}|_E &= \frac{1}{|E|}\int_E q \,\mathrm{dx} \qquad \forall\, E \in \mathcal{T}_h \quad \forall\, q \in L^1(\Omega), \\ \mathbf{G}^{\mathrm{I}}|_{\mathsf{e}} &= \frac{1}{|\mathsf{e}|}\int_{\mathsf{e}} G \cdot \mathbf{n}^{\mathsf{e}} \,\mathrm{ds} \quad \forall\, \mathsf{e} \in \mathcal{E}_h \quad \forall\, G \in H(\mathrm{div}, \Omega), \end{aligned} \tag{21}$$

where, for any edge $\mathsf{e} \in \mathcal{E}_h$, $\mathbf{n}^{\mathsf{e}}$ is a unit normal vector assigned to e once and for all, see [33]. We also define the mimetic discrete divergence operator $\mathcal{DIV}_h : \mathbf{W}^h \to Q^h$ as

$$(\mathcal{DIV}_h\, \mathbf{G})\,|_E = \frac{1}{|E|}\sum_{\mathsf{e}\subseteq\partial E} |\mathsf{e}| G_E^{\mathsf{e}} \quad \forall E \in \mathcal{T}_h, \tag{22}$$

where $G_E^{\mathsf{e}} = G^{\mathsf{e}}\mathbf{n}^{\mathsf{e}} \cdot \mathbf{n}_E^{\mathsf{e}} \in \mathbb{R}$, being $\mathbf{n}_E^{\mathsf{e}}$ the unit vector normal to e pointing out of E. This definition is consistent with the Gauss divergence theorem. We also recall that it holds,

$$(\mathrm{div}\, G)^{\mathrm{I}} = \mathcal{DIV}_h(\mathbf{G}^{\mathrm{I}}),$$

cf. [30] for details.

Next, we define suitable scalar products onto the discrete spaces Q^h and $\mathbf{W}^h$. On Q^h we set

$$[\boldsymbol{p}, \boldsymbol{q}]_{Q^h} = \sum_{E\in\mathcal{T}_h} |E| p_E q_E \qquad \forall\, \boldsymbol{p}, \boldsymbol{q} \in Q^h, \tag{23}$$

which corresponds to the $L^2(\Omega)$ scalar product for piecewise constant functions. The scalar product in $\mathbf{W}^h$ is defined by assembling elementwise contributions from each element, *i.e.*,

$$[\mathbf{F}, \mathbf{G}]_{\mathbf{W}^h} = \sum_{E\in\mathcal{T}_h} [\mathbf{F}, \mathbf{G}]_E \qquad \forall\, \mathbf{F}, \mathbf{G} \in \mathbf{W}^h, \tag{24}$$

where, by following [29, 30], the local scalar product $[\cdot, \cdot]_E$ can be defined in such a way that the following two conditions are satisfied:

(S1) *Stability*: for all $\mathbf{G} \in \mathbf{W}^h$ and for every element $E \in \mathcal{T}_h$ it holds

$$\sum_{\mathsf{e}\subseteq\partial E} |E| (G_E^{\mathsf{e}})^2 \lesssim [\mathbf{G}, \mathbf{G}]_E \lesssim \sum_{\mathsf{e}\subseteq\partial E} |E| (G_E^{\mathsf{e}})^2;$$

(S2) *Local consistency*: for every linear function q^1 on $E \in \mathcal{T}_h$ it holds

$$[(\mathbf{K}^E \nabla q^1)^{\mathrm{I}}, \mathbf{G}]_E + \int_E q^1\, \mathcal{DIV}_h\, \mathbf{G} \,\mathrm{dx} = \sum_{\mathsf{e}\subseteq\partial E} G_E^{\mathsf{e}} \int_{\mathsf{e}} q^1 \,\mathrm{ds}$$

for all $\mathbf{G} \in \mathbf{W}^h$, where $\mathbf{K}^E$ is a constant permeability tensor approximation to $\mathbf{K}$ on E such that $\|\mathbf{K}^E - \mathbf{K}\|_{L^\infty(E)} \lesssim h_E$, where the hidden constant is independent of E.

We are now ready to state the mimetic discretization of problem (7a)-(7b) under the assumption that p_Γ is given. To this aim let

$$p_{\Gamma,i} \simeq \frac{1}{|\hat{\mathsf{e}}_i|}\int_{\hat{\mathsf{e}}_i} p_\Gamma \,\mathrm{ds}, \tag{25}$$

be the approximation of the fracture pressure in $\hat{\mathsf{e}}_i$ that will be computed by a finite volume scheme, as explained in the next section. Then our formulation reads as: find $\mathbf{F}_h \in \mathbf{W}^h_{0,\Gamma_\mathrm{N}}$ and $\boldsymbol{p}_h \in Q^h$ such that

$$\begin{cases} [\mathbf{F}_h, \mathbf{G}]_{\mathbf{W}^h} - [\boldsymbol{p}_h, \mathcal{DIV}_h\,\mathbf{G}]_{Q^h} + [\mathbf{F}_h, \mathbf{G}]_\Gamma + \displaystyle\sum_{i=1}^{N_\Gamma} |\hat{\mathsf{e}}_i| [\![\mathbf{G}]\!]_{\hat{\mathsf{e}}_i}\; p_{\Gamma,i} = \mathcal{L}_h(\mathbf{G}) \quad \forall\, \mathbf{G} \in \mathbf{W}^h_{0,\Gamma_\mathrm{N}}, \\ \qquad\qquad [\mathcal{DIV}_h\,\mathbf{F}_h, \boldsymbol{q}]_{Q^h} = \mathcal{G}_h(\boldsymbol{q}_h) \quad \forall\, \boldsymbol{q} \in Q^h, \end{cases} \tag{26}$$

with

$$[\mathbf{F}_h, \mathbf{G}]_\Gamma = \sum_{j=1}^{2}\sum_{i=1}^{N_\Gamma} \eta_\Gamma \left(\xi \mathbf{F}_h^{\mathsf{e}^i_j} - (1-\xi)\mathbf{F}_h^{\mathsf{e}^i_{j+1}}\right) \mathbf{G}^{\mathsf{e}^i_j},$$

where the index j varies in $\mathbb{Z}/2\mathbb{Z}$. The right hand sides in (26) are defined as

$$\begin{aligned} \mathcal{L}_h(\mathbf{G}) &= \sum_{\mathsf{e}\in\mathcal{E}_h^{\Gamma_{\mathrm{D},1}}\cup\mathcal{E}_h^{\Gamma_{\mathrm{D},2}}} |\mathsf{e}| G^{\mathsf{e}} g_\mathrm{D}^{\mathsf{e}}\ , && \forall\, \mathbf{G} \in \mathbf{W}^h_{0,\Gamma_\mathrm{N}} \\ \mathcal{G}_h(\boldsymbol{q}) &= [\mathbf{f}, \boldsymbol{q}]_{Q^h}, && \forall\, \boldsymbol{q} \in Q^h, \end{aligned}$$

where

$$g_\mathrm{D}^{\mathsf{e}} = \frac{1}{|\mathsf{e}|}\int_{\mathsf{e}} g_\mathrm{D}\,\mathrm{ds},$$

and $\mathbf{f} = \mathbf{f}^\mathrm{I}$ is the vector of the mean values of f, defined according to (21).

4.2. **Finite volume discretization of the fracture problem**

To discretize (5) we employ a finite volume formulation. We consider the partition Γ_h of Γ induced by the mimetic discretization introduced in the previous section and we set $h_{\Gamma,i} = |\hat{\mathsf{e}}_i| > 0$ and set $h_\Gamma = \max_i h_{\Gamma,i}$. We consider a parametric description of Γ_h and indicate with s the arc-length coordinate. We assume to have numbered the fracture edges so that s_i is the center of $\hat{\mathsf{e}}_i$, with $s_1 < s_2 < \ldots < s_{N_\Gamma}$, and $s_{i-1/2}$ and $s_{i+1/2}$ are the two end points of $\hat{\mathsf{e}}_i$. Clearly, $h_{\Gamma,i} = s_{i+1/2} - s_{i-1/2}$. If we consider an edge $\hat{\mathsf{e}}_i$ fully contained in Γ_h, *i.e.*, with $i \in \{2, \ldots, N_\Gamma - 1\}$, the integration of the differential equation in (5) over $\hat{\mathsf{e}}_i$ gives

$$\kappa_\Gamma \nabla_\tau p_\Gamma|_{s_{i-1/2}} - \kappa_\Gamma \nabla_\tau p_\Gamma|_{s_{i+1/2}} = \int_{\hat{\mathsf{e}}_i} (\ell_\Gamma f_\Gamma + [\![\mathbf{u}\cdot\mathbf{n}_\Gamma]\!])\,\mathrm{ds}. \tag{27}$$

We define $\boldsymbol{p}_{\Gamma,h} = \{p_{\Gamma,1}, \ldots p_{\Gamma,N_\Gamma}\} \in Q^h_\Gamma = \mathbb{R}^{N_\Gamma}$ where $p_{\Gamma,i}$ is given in (25). As explained in the previous section, for each $\hat{\mathsf{e}}_i$ we have two duplicated edges $\mathsf{e}^1_1 \in \mathcal{E}^\Gamma_{h,1}$ and $\mathsf{e}^2_2 \in \mathcal{E}^\Gamma_{h,2}$, and the jump defined as in (20) is constant in $\hat{\mathsf{e}}_i$. We assume that also κ_Γ is piecewise constant, with values $\{\kappa_i,\, i = 1, \ldots N_\Gamma\}$, and we set $f_i = |\hat{\mathsf{e}}_i|^{-1}\int_{\hat{\mathsf{e}}_i} \ell_\Gamma f_\Gamma\,\mathrm{ds}$.

For $i = 1, \ldots N_\Gamma - 1$ we introduce the numerical fluxes $H_{i+1/2} \simeq u_{i+1/2} = -\kappa_\Gamma \nabla_\tau p_\Gamma|_{s_{i+1/2}}$. In particular, we consider the so-called two-point flux approximation, where

$$H_{i+1/2}(a,b) = T_{i+1/2}(a-b),$$

being $T_{i+1/2}$ the so-called transmissibility between $\hat{\mathsf{e}}_i$ and $\hat{\mathsf{e}}_{i+1}$. To evaluate it, let us first consider the case where $\hat{\mathsf{e}}_i$ and $\hat{\mathsf{e}}_{i+1}$ lie on a straight segment. Since the velocity is well defined at the interface, we have $u_{i+1/2} = -\kappa_\Gamma(s^-_{i+1/2})\nabla_\tau p_\Gamma(s^-_{i+1/2}) = -\kappa_\Gamma(s^+_{i+1/2})\nabla_\tau p_\Gamma(s^+_{i+1/2})$. Note that, since κ_Γ and $\nabla_\tau p_\Gamma$ may be discontinuous

across elements, we are here taking the left and right limits. Assuming that $\nabla_\tau p_\Gamma$ is continuous on each cell, by performing a Taylor expansion around $s_{i+1/2}$ in $\hat{\mathbf{e}}_i$ and $\hat{\mathbf{e}}_{i+1}$, respectively, we obtain

$$\begin{array}{ll} u_{i+1/2} & = \frac{2\kappa_i}{h_i}(p_i - p_{i+1/2}) + o(h_\Gamma) \\ u_{i+1/2} & = \frac{2\kappa_{i+1}}{h_{i+1}}(p_{i+1/2} - p_{i+1}) + o(h_\Gamma), \end{array} \tag{28}$$

where $p_i = p_\Gamma(s_i)$. By manipulating the two expressions to eliminate $p_{i+1/2}$, neglecting the $o(h_\Gamma)$ term, and recalling that $H_{i+1/2}$ is an approximation of $u_{i+1/2}$, we derive the following expression for the trasmissibility

$$T_{i+1/2} = \frac{\alpha_i \alpha_{i+1}}{\alpha_i + \alpha_{i+1}}, \tag{29}$$

with

$$\alpha_i = \frac{2\kappa_i}{h_i}. \tag{30}$$

Note that if p_Γ has continuous second derivative on each cell then the formula for the numerical fluxes is in fact second order accurate with respect to h_Γ. Indeed, in this case when eliminating $p_{i+1/2}$ the term of order h_Γ in (28) cancels out, leaving a remainder of higher order. If $\hat{\mathbf{e}}_i$ and $\hat{\mathbf{e}}_{i+1}$ form an angle $\zeta_{i+1/2}$, we modify (30) according to the recipe suggested in [44], and replace (29) with

$$T_{i+1/2} = \frac{\alpha_i \alpha_{i+1}}{\alpha_i + \alpha_{i+1}} \cos(\frac{\zeta_{i+1/2}}{2}).$$

In view of the above discussion, equation (27) is then approximated by

$$H_{i-1/2}(p_{\Gamma,i}, p_{\Gamma,i-1}) + H_{i+1/2}(p_{\Gamma,i}, p_{\Gamma,i+1}) - h_{\Gamma,i}[\![\mathbf{F}_h]\!]_{\hat{\mathbf{e}}_i} = h_{\Gamma,i} f_i, \tag{31}$$

for $i = 2, \dots N_\Gamma - 1$, where we have also moved the jump term on the left hand side.

We have now to handle the boundary cells. If a boundary cell is adjacent to $\partial\Gamma_N$ we still use (31), but we set to zero the numerical flux at the corresponding cell boundary. For a Dirichlet condition, we use again a Taylor expansion. If, without loss of generality, we assume that $\hat{\mathbf{e}}_1$ is adjacent to $\partial\Gamma_D$, the resulting equation is

$$\alpha_1 p_1 + H_{3/2}(p_{\Gamma,1}, p_{\Gamma,2}) - h_{\Gamma,1}[\![\mathbf{F}_h]\!]_{\hat{\mathbf{e}}_1} = h_{\Gamma,1} f_1 + \alpha_1 g_D. \tag{32}$$

In the case of networks of fractures we have to cope with the intersection of three or more fractures. Each fracture is meshed independently and we have $|\mathcal{S}_i|$ cells that meet at intersection i, corresponding to the fractures intersecting at that point. For simplicity (and no loss of generality), let us call them $\hat{\mathbf{e}}_{\gamma_k,i}$, with $\gamma_k \in \mathcal{S}_i$, and indicate with $\alpha_{\gamma_k,i}$ the corresponding coefficient computed according to (30). The transmissibility coefficient T_{kj} for the degrees of freedom associated to $C_{\gamma_k,i}$ and $C_{\gamma_j,i}$, with $\gamma_k, \gamma_j \in \mathcal{S}_i$, is now

$$T_{kj} = \frac{\alpha_{\gamma_k,i}\alpha_{\gamma_j,i}}{\sum_{\gamma_s \in \mathcal{S}_i} \alpha_{\gamma_s,i}} \cos(\frac{\zeta_{kj}}{2}), \tag{33}$$

being ζ_{kj} the angle between γ_k and γ_j at the intersection. Clearly $T_{kj} = T_{jk}$.

4.3. **Fully-coupled problem and its algebraic formulation**

Let N_f, N_p be the dimensions of the discrete spaces $\mathbf{W}^h$ and Q^h, respectively, and recall that N_Γ is the number of edges belonging to Γ_h. The final algebraic system stemming from the mimetic/finite volume

discretization has a saddle point structure. Indeed, problem (26) is algebraically equivalent to

$$\begin{aligned} \mathrm{A}\mathbf{F}_h + \mathrm{B}^T \boldsymbol{p}_h + \mathrm{C}^T \boldsymbol{p}_{\Gamma,h} &= \mathbf{b}_F \\ \mathrm{B}\mathbf{F}_h &= \mathbf{b}_p, \end{aligned}$$

where $\mathrm{A} \in \mathbb{R}^{N_f \times N_f}$ is the matrix representing the linear operator $[\mathbf{F}_h, \mathbf{G}]_{\mathbf{W}^h} + [\mathbf{F}_h, \mathbf{G}]_\Gamma$, while $\mathrm{B}^T \in \mathbb{R}^{N_f \times N_p}$ and $\mathrm{C}^T \in \mathbb{R}^{N_f \times N_\Gamma}$ represent the terms $-[\boldsymbol{p}_h, \mathcal{DIV}_h \mathbf{G}]_{Q^h}$ and $\sum_{i=1}^{N\Gamma} |\hat{\mathrm{e}}_i| [\![\mathbf{G}]\!]_{\hat{\mathrm{e}}_i} \, p_{\Gamma,i}$, respectively. Finally, $\mathbf{b}_f$ and $\mathbf{b}_p$ collect the contributions to the right hand side (we have changed the sign in discrete divergence equation to recover the classical matrix structure for saddle point problems). Since the grid used for the fracture problem is conforming to the mimetic grid, it is immediate to recognize that assembling (31) and (32) and using the given definitions of the numerical flux produces the linear system

$$\mathrm{C}\mathbf{F}_h - \mathrm{T}\boldsymbol{p}_{\Gamma,h} = \mathbf{b}_\Gamma, \tag{34}$$

where $T \in \mathbb{R}^{N_\Gamma \times N_\Gamma}$ assembles all the transmissibility terms, and $\mathbf{b}_\Gamma$ collects all contributions to the right hand side due to the forcing term and Dirichlet boundary data. We can then write

$$\begin{bmatrix} \mathrm{A} & \mathrm{B}^T & \mathrm{C}^T \\ \mathrm{B} & 0 & 0 \\ \mathrm{C} & 0 & -\mathrm{T} \end{bmatrix} \begin{bmatrix} \mathbf{F}_h \\ \boldsymbol{p}_h \\ \boldsymbol{p}_{\Gamma,h} \end{bmatrix} = \begin{bmatrix} \mathbf{b}_F \\ \mathbf{b}_p \\ \mathbf{b}_\Gamma \end{bmatrix}. \tag{35}$$

Now, thank to the hypothesis on Γ_D, the matrix A is symmetric and positive definite, while B^T has zero null-space because of the inf-sup condition, cf. Proposition 2.2. Furthermore, we have the following result.

Proposition 4.1. *Let*

$$\widetilde{\mathrm{C}}^T = \begin{bmatrix} \mathrm{B}^T & \mathrm{C}^T \end{bmatrix} \in \mathbb{R}^{N_f \times (N_p + N_\Gamma)}. \tag{36}$$

Then, $\ker(\mathrm{C}^T) = \{\mathbf{0}\}$ *and* $\ker(\widetilde{\mathrm{C}}^T) = \{\mathbf{0}\}$.

Proof. For a $\boldsymbol{p}_{\Gamma,h} \in \mathbb{R}^{N_\Gamma}$ we have that $\mathbf{G}\mathrm{C}^T \boldsymbol{p}_{\Gamma,h} = \sum_{i=1}^{N_\Gamma} |\hat{\mathrm{e}}_i| [\![\mathbf{G}]\!]_{\hat{\mathrm{e}}_i} \, p_{\Gamma,i}$. For any $\boldsymbol{p}_{\Gamma,h} \neq \mathbf{0}$ it is sufficient to choose a $\mathbf{G}$ such that $[\![\mathbf{G}]\!]_{\hat{\mathrm{e}}_i} = p_{\Gamma,i}$ to have $\mathbf{G}_h \mathrm{C}^T \boldsymbol{p}_{\Gamma,h} > 0$ and thus $\mathrm{C}^T \boldsymbol{p}_{\Gamma,h} \neq \mathbf{0}$, *i.e.*, $\ker(\mathrm{C}^T) = \{\mathbf{0}\}$. We now note that the operator B from $\mathbf{W}^h_{0,\Gamma_\mathrm{N}}$ to Q^h such that $\boldsymbol{q}_h = \mathrm{B}\mathbf{G}$ for every $\mathbf{G} \in \mathbf{W}^h_{0,\Gamma_\mathrm{N}}$ is still surjective even when restricted to the subspace $\widetilde{\mathbf{W}}^h_{0,\Gamma_\mathrm{N}} = \{\mathbf{G} \in \mathbf{W}^h_{0,\Gamma_\mathrm{N}} : \; [\![\mathbf{G}]\!]_{\hat{\mathrm{e}}_i} = 0 \quad \forall i\}$. Indeed, imposing a zero jump on the velocity is equivalent to applying the discrete divergence operator to a standard Darcy field on Ω without fractures, and for this case we can use standard results on mimetic finite differences. This observation implies that, by setting $\widetilde{N}_f = \dim(\widetilde{\mathbf{W}}^h_{0,\Gamma_\mathrm{N}})$ for any $\mathbf{0} \neq \boldsymbol{q}_h \in \mathbb{R}^{N_p}$, we may find a $\mathbf{G} \in \mathbb{R}^{\widetilde{N}_f}$ such that $\boldsymbol{q}_h = \mathrm{B}\mathbf{G}$, and thus $\mathbf{G}^T \mathrm{B}^T \boldsymbol{q}_h = \|\boldsymbol{q}_h\|^2 > 0$, being $\|\cdot\|$ the standard Euclidean norm. Furthermore, for such a $\mathbf{G}$ we have that $\mathbf{G}^T \mathrm{C}^T \boldsymbol{q}_h = 0$. Consequently, for any $\widetilde{\boldsymbol{q}}_h = [\boldsymbol{q}_h^T, \boldsymbol{q}_{\Gamma,h}^T]^T \in \mathbb{R}^{N_p \times N_\Gamma}$ different from zero we may consider the following two cases. If $\boldsymbol{q}_h \neq \mathbf{0}$ then we can select a $\mathbf{G} \in \widetilde{\mathbf{W}}^h_{0,\Gamma_\mathrm{N}}$ such that $\mathbf{G}^T \widetilde{\mathrm{C}}^T \widetilde{\boldsymbol{q}}_h = \mathbf{G}^T \mathrm{B}^T \boldsymbol{q}_h > 0$. If instead $\boldsymbol{q}_h = \mathbf{0}$ then $\mathbf{G}^T \widetilde{\mathrm{C}}^T \widetilde{\boldsymbol{q}}_h = \mathbf{G}^T \mathrm{C}^T \boldsymbol{q}_\Gamma$ and we can exploit the previous result on the kernel of C^T. Consequently, $\ker(\widetilde{\mathrm{C}}^T) = \{\mathbf{0}\}$. □

We next show a result on the transmissibility matrix T that we will need later on.

Proposition 4.2. *The matrix T is symmetric and semipositive definite (with kernel formed by constant vectors) if $\partial\Gamma_D = \emptyset$. Moreover, if $\partial\Gamma_D \neq \emptyset$, then* T *is positive definite.*

Proof. It can be verified that, by construction, the matrix T is symmetric and is a Z-matrix with positive diagonal elements.

If $\partial\Gamma_D = \emptyset$ we have that $\mathrm{T}_{ii} = -\sum_j \mathrm{T}_{ij}$ for all i, so it is diagonally dominant with the vector $[1, 1, \ldots, 1]^T$ in the kernel. Otherwise, at the Dirichlet end points equation(32) implies that at least one row i satisfies $\mathrm{T}_{ii} > \sum_j |\mathrm{T}_{ij}|$. The thesis then follows from standard linear algebra results. □

The next result shows that the linear system (35) admits a unique solution.

Proposition 4.3. *The linear system* (35) *admits a unique solution.*

Proof. We can exploit a well known result for saddle point problems [18]. Indeed, we can reformulate the governing matrix in (35) as

$$\mathrm{K} = \begin{bmatrix} \mathrm{A} & \widetilde{\mathrm{C}}^T \\ \widetilde{\mathrm{C}} & -\widetilde{\mathrm{T}} \end{bmatrix},$$

where

$$\widetilde{\mathrm{T}} = \begin{bmatrix} 0 & 0 \\ 0 & \mathrm{T} \end{bmatrix}$$

is symmetric and semipositive definite, cf. Proposition 4.2, and $\widetilde{\mathrm{C}}$ has been defined as in (36). Then, K is non-singular if and only if $\ker(\widetilde{\mathrm{C}}^T) \cap \ker(\widetilde{\mathrm{T}}) = \{\mathbf{0}\}$. This is automatically satisfied since $\ker(\widetilde{\mathrm{C}}^T) = \{\mathbf{0}\}$ because of Proposition 4.1. □

Remark 4.1. *Note that to prove the well-posedness at the continuous level, we assumed that $\partial\Gamma_D \neq \emptyset$, cf. Section 2. From the analysis of the discrete problem, we can conjecture that this condition can be relaxed and that the coupling conditions are sufficient to guarantee the existence of a unique discrete solution. Indeed, the well-posedness for the problem with a single immersed fracture, where no Dirichlet conditions are imposed on the fracture, has been already obtained in [4], even if by using a different formulation.*

Remark 4.2. *In the case of networks of fractures the resulting algebraic system is still of the form* (35)*.*

5. Numerical results

In this section we describe the numerical results obtained by employing the previously discussed models. The numerical models have been implemented in a software written in `C++` language. For the generation of the meshes we have used of the `CGAL` library [51], while for matrix manipulation and linear system solution we exploited the `Eigen` library [41].

Throughout this section the parameter ξ appearing in the definition (6) of the coupling conditions has been chosen as $\xi = 0.75$. Moreover, the fracture thickness has been set equal to $\ell_\Gamma = 0.01$.

5.1. Example 1

The first test case is based on the example proposed in [42], with slight modifications. We take $\Omega = (-1, 1) \times (-1, 1)$, $\Gamma = (-1, 1) \times \{0\}$ and impose homogeneous Dirichlet boundary conditions on the whole boundary of Ω, *i.e.*, $\Gamma_\mathrm{N} = \emptyset$ and $\Gamma_\mathrm{D} = \partial\Omega$; the boundary conditions for the fracture problem are imposed accordingly. The bulk permeability tensor is assumed to be the identity matrix, *i.e.*, $\mathbf{K} = \mathbf{I}$, whereas the fracture permeability tensor is chosen as $\mathbf{K}_\Gamma = \varepsilon\mathbf{I}$, for a positive real number ε that will be specified later on. Notice that, according to the definition given in (4), the permeability of the reduced model (5) is given by $\kappa_\Gamma = \ell_\Gamma\varepsilon$. Moreover, with the above choice of $\mathbf{K}_\Gamma$ the parameter η_Γ appearing in the coupling conditions (6) becomes $\eta_\Gamma = \ell_\Gamma/\varepsilon$. We take the source terms as

$$f(x, y) = (1 - \varepsilon)\cosh(\frac{\ell_\Gamma}{2})\cos(x) \qquad \text{in } \Omega,$$

$$f_\Gamma(x) = \varepsilon^2\cos(x) + \varepsilon(1 - \varepsilon)\cosh(\frac{\ell_\Gamma}{2})\cos(x) \quad \text{on } \Gamma,$$

	$\varepsilon = 0.001$		$\varepsilon = 1$		$\varepsilon = 1000$	
	Grid I	Grid II	Grid I	Grid II	Grid I	Grid II
Rate of convergence, pressure	1.8770	1.9867	1.7440	1.6752	1.8362	1.8906
Rate of convergence, velocity	1.4535	1.0461	1.2266	1.0597	1.4567	1.0739

TABLE 1. Example 1. Mean convergence rates for $\varepsilon = 0.001, 1, 1000$.

so that the exact solution is given by

$$\begin{cases} p = \varepsilon \cos(x)\cosh(y) + (1-\varepsilon)\cosh(\frac{\ell_\Gamma}{2})\cos(x) & \text{in } \Omega, \\ p_\Gamma = \varepsilon \cos(x) + (1-\varepsilon)\cosh(\frac{\ell_\Gamma}{2})\cos(x) & \text{on } \Gamma. \end{cases}$$

We have tested our numerical scheme on a sequence of unstructured triangular (Grid I) and polygonal grids (Grid II) with granularity $h \approx 1/N$ for $N = 2, 4, 8, 16, 32, 64$. Any polygonal decomposition has been obtained from a triangular grid by merging randomly two or more triangles leading then to a decomposition containing elements that can have three, four or five edges, cf. Figure 3(a) for an example.

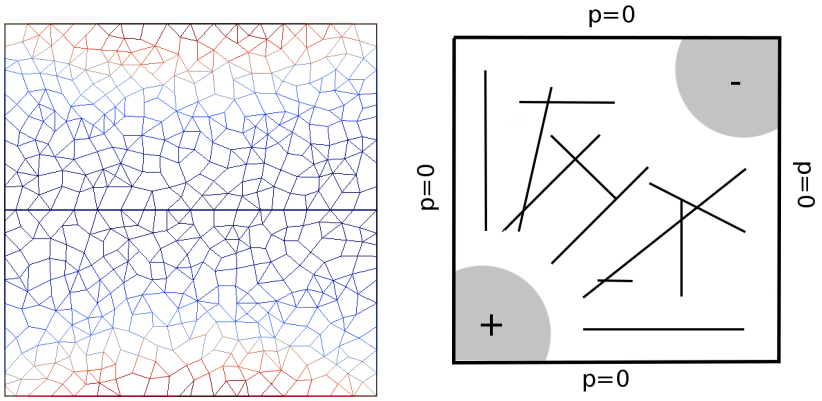

(a) Example 1 (b) Example 3

FIGURE 3. Left: Computational domain and its polygonal decomposition for Example 1. Right: Computational domain and boundary conditions for Example 3.

We measure the relative approximation errors for the pressure and the velocity in the bulk domain as:

$$\text{err}_p = \frac{\|p^I - p_h\|_{Q^h}}{\|p^I\|_{Q^h}}, \qquad \text{err}_v = \frac{\|\mathbf{u}^I - \mathbf{u}_h\|_{\mathbf{W}^h}}{\|\mathbf{u}^I\|_{\mathbf{W}^h}},$$

where p^I and $\mathbf{u}^I$ are the interpolants of the exact solution (pressure and velocity) in the mimetic spaces Q^h and $\mathbf{W}^h$, respectively. In Figure 4 we report the computed relative errors err_p and err_v as a function of the meshsize (loglog scale) for $\varepsilon = 0.001, 1, 1000$. The results reported in Figure 4 clearly show that a second order convergence rate for the pressure variable is clearly achieved; this superconvergence effect has been already observed in many cases, see [32] and [14] for examples. As concerns velocity we have at least first order convergence in all cases. The mean convergence rates are summarized in Table 1.

5.2. **Example 2**

In this second test case we investigate the robustness of our scheme with respect to the contrasts between the permeability in the bulk and in the fracture. We let $\Omega = (0,1) \times (0,1)$. On $\Gamma_D = \{0,1\} \times (0,1)$ we impose

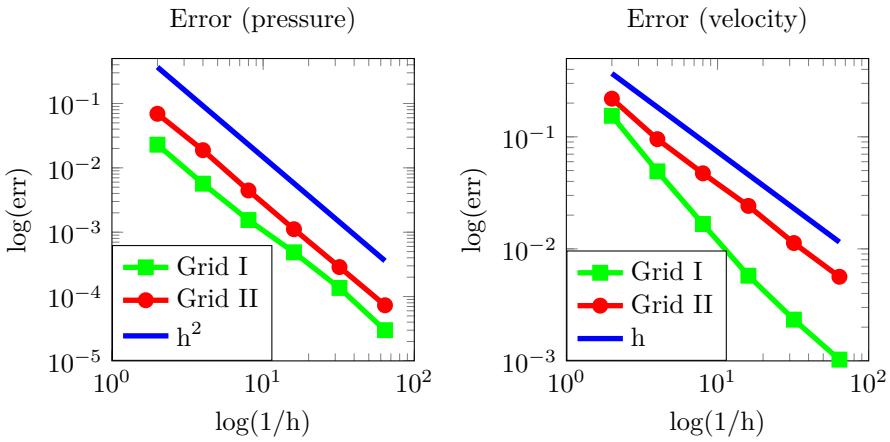

(a) $\varepsilon = 0.001$

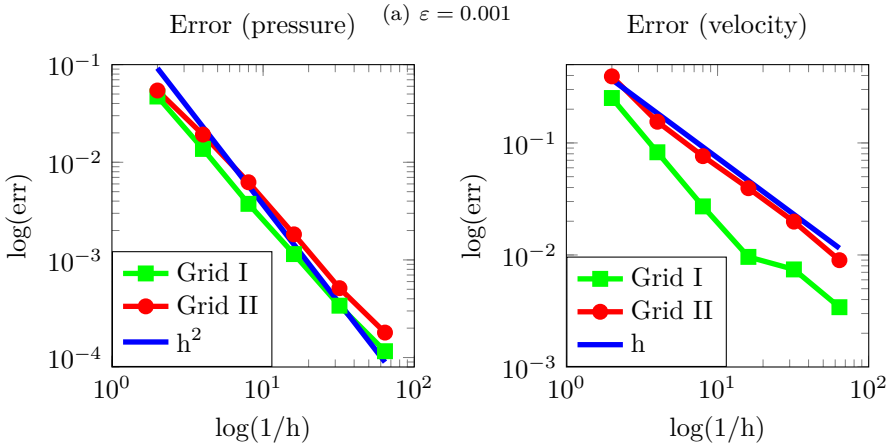

(b) $\varepsilon = 1$

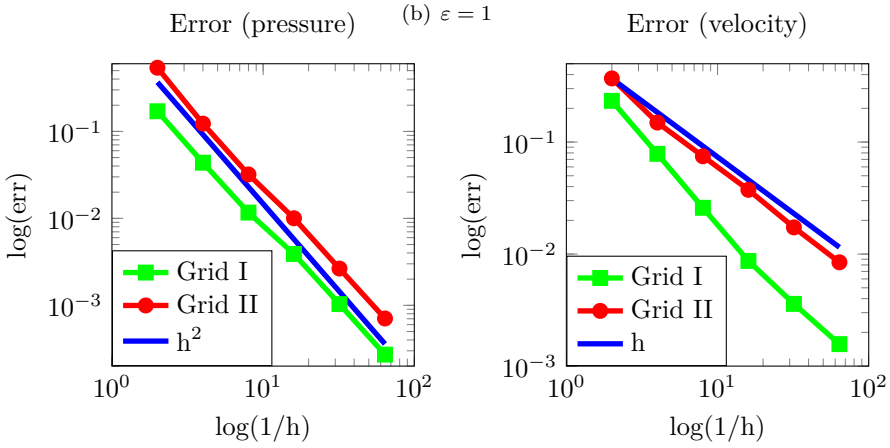

(c) $\varepsilon = 1000$

FIGURE 4. Example 1. Computed relative errors as a function of the meshsize (loglog scale) for $\varepsilon = 0.001, 1, 1000$.

a non-homogeneous Dirichlet condition $g_D = y$ whereas on $\Gamma_N = [0,1] \times \{0,1\}$ we impose a homogeneous condition, *i.e.*, $g_N = 0$. The right hand side is chosen as $f(x,y) = 4$ in Ω. The fracture is given by $\Gamma = \{(x,y) \in \Omega : y + 2x = 1.4\}$. We take the medium to be isotropic and set $\mathbf{K} = \mathbf{I}$, and let the parameters κ_Γ^n and κ_Γ^τ vary. Note that κ_Γ^n and κ_Γ^τ completely determine the permeability of the fracture and therefore its behavior when embedded in the porous medium. We have considered the following cases:

i) $\kappa_\Gamma^\tau = 1$, $\kappa_\Gamma^n = 1$. In this case the pressure is expected to be almost constant across the fracture Γ because the permeability in the normal direction is equal to that of the surrounding medium and the fluid is not affected by the presence of the fracture. This is exactly the behavior observed in Figure 5(a);

ii) $\kappa_\Gamma^\tau = 1$, $\kappa_\Gamma^n = 0.01$. Here the normal permeability is smaller than that of the surrounding medium, therefore we expect a pressure jump across the fracture, cf. Figure 5(b) where this behavior is clearly observed;

iii) $\kappa_\Gamma^\tau = 100$, $\kappa_\Gamma^n = 1$. In this case the fracture pressure is expected to be almost linear and the flow is expected to be directed towards the fracture. This because here the fracture is very permeable in the tangential direction and the fluid is "attracted" by the fracture. This is exactly the behavior observed in Figure 5(c).

In all the aforementioned cases we compare the result obtained with the mimetic method with the analogous ones computed with the XFEM approach described in [34] where a mixed finite element formulation is combined with a suitable enrichment on the elements crossed by the fracture. As shown in Figure 5 the results obtained with the two methods are in good agreement in all the cases. Meshes with a similar size h have been used in the two approaches: for the mimetic method we use a polygonal grid obtained with the agglomeration of a constrained Delaunay triangulation, while for the XFEM, since we do not need to honor the fracture geometry, we use a structured triangular grid.

5.3. **Example 3**

In this example we aim at assessing the proposed scheme on a more complex network of fractures. We compare the solution of our scheme with a discretization where finite volumes have been employed to discretize both the bulk as well as the fracture equations. We choose a domain $\Omega = (0,1) \times (0,1)$ containing 10 fractures, see Figure 3(b). The finite volume scheme adopted employs a simple two-point flux approximation. It is known that this scheme can be unaccurate unless special grids are employed. In particular, a sufficient condition for the consistency of two-point flux approximation for an isotropic permeability tensor requires that the normal to any interior edge be directed along the segments joining the centroids of the adjacent elements. To satisfy this requirement as far as possible for the finite volume scheme we have generated the grid using the constrained Delaunay triangulation tool of the CGAL library. For more information on the finite volume method, the interested reader may consult [39], or the recent review [35]. We set homogeneous Dirichlet boundary conditions on the whole boundary of Ω and set the source term

$$f(x,y) = \begin{cases} 10 & \text{per } (x-0.1)^2 + (y-0.1)^2 \leq 0.04 \\ -10 & \text{per } (x-0.9)^2 + (y-0.9)^2 \leq 0.04 \end{cases},$$

that represents a source in the lower left corner of Ω and a sink in the top right corner. Finally, for simplicity we consider an isotropic and homogeneous porous medium, *i.e.*, $\mathbf{K} = \mathbf{I}$ as well as isotropic fractures, *i.e.*, $\mathbf{K}_\Gamma = \varepsilon \mathbf{I}$, where ε can vary. We have considered the following test cases: *i)* no fractures (Figure 6(a)); *ii)* $\varepsilon = 1000$ (Figure 6(b)); and *iii)* $\varepsilon = 0.001$ (Figure 6(c)). The corresponding discrete pressures computed with the mimetic finite difference scheme are reported in Figure 6 (left) and the analogous results obtained with the finite volume method are shown in Figure 6 (right). From these results we can conclude that in all the cases the results produced by mimetic finite differences are consistent with those obtained employing finite volumes. Even when no fractures are present in the domain, the solution computed with the finite volume method seems to exhibit higher pressure peaks than those obtained with mimetic finite differences, cf. Figure 6(a). This might be due to the fact that on grids of similar density the two-point finite volume method considered here is less accurate and tends to produce smaller transmissibility. It is not the scope of this work to analyze this matter

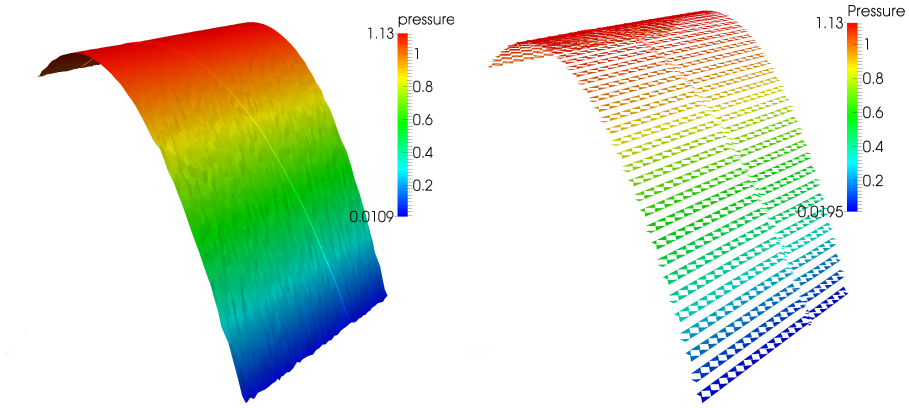

(a) $\kappa_\Gamma^\tau = 1$, $\kappa_\Gamma^n = 1$, with MFD (left) and XFEM (right)

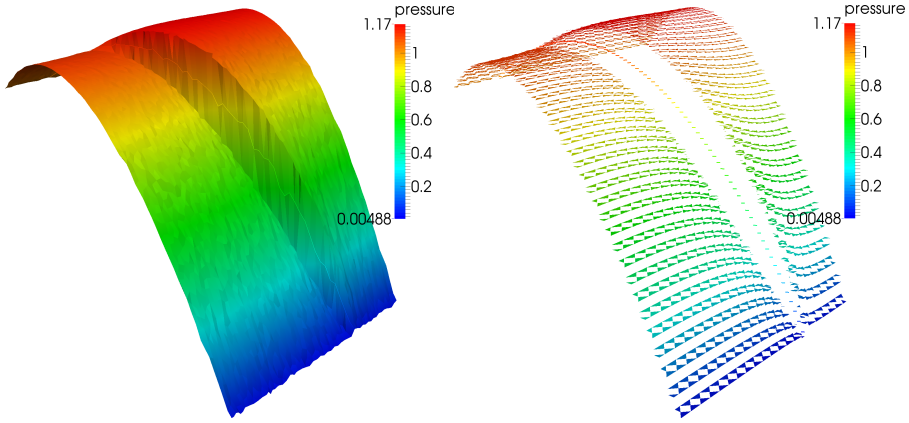

(b) $\kappa_\Gamma^\tau = 1$, $\kappa_\Gamma^n = 0.01$, with MFD (left) and XFEM (right)

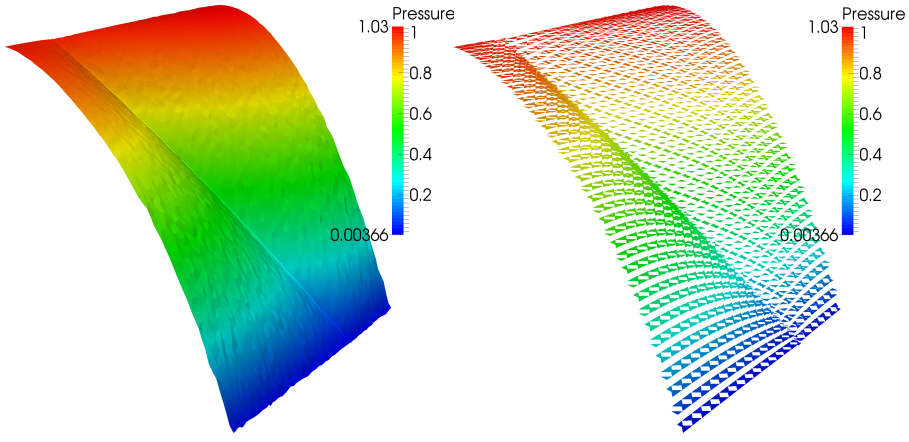

(c) $\kappa_\Gamma^\tau = 100$, $\kappa_\Gamma^n = 1$, with MFD (left) and XFEM (right)

FIGURE 5. Example 2. Computed pressure for different choices of the permeability coefficients κ_Γ^n and κ_Γ^τ that characterize the fracture.

in more detail, since we are showing this example just to illustrate the suitability of the proposed scheme also in the case of networks of fractures.

If $\varepsilon = 1000$ the fractures are much more permeable than the surrounding medium. Indeed, pressure is practically continuous across the fractures and the maximum and minimum values of pressure are slightly lower with respect to the non-fractured case, both for mimetic finite differences and finite volumes. Finally, if $\varepsilon = 0.001$, *i.e.*, the fractures are much less permeable than the bulk and we can observe strong pressure jumps across fractures. Once again, finite volume predicts higher peaks with respect to the mimetic finite difference method but the solutions are in good agreement.

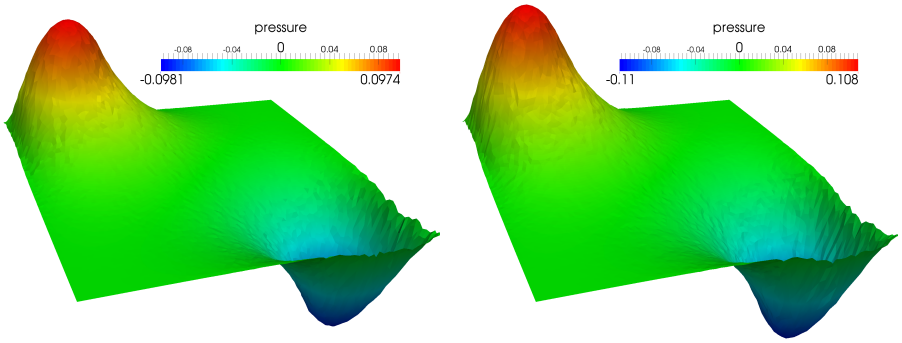

(a) No fractures

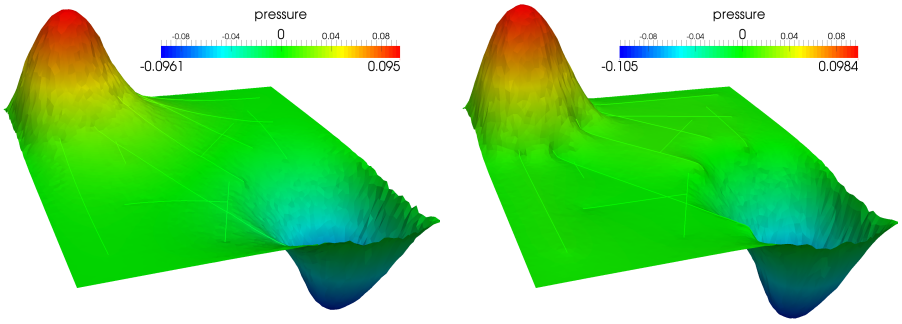

(b) Fracture configuration given in Figure 3(b), $\varepsilon = 1000$

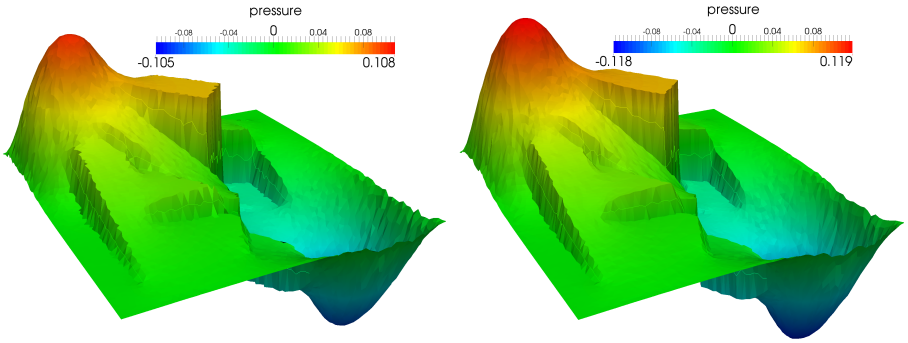

(c) Fracture configuration given in Figure 3(b), $\varepsilon = 0.001$

FIGURE 6. Example 3. Mimetic finite difference (left) and finite volume (right) computed pressures for different geometrical configurations and different choices of ε.

6. Conclusions

In this paper we have presented a possible framework for the numerical simulation of flow in fractured porous media, by coupling mimetic finite differences for the porous matrix with a model of the flow in the fractures based on a pressure formulation and a finite volume scheme. The reason for using different formulations for bulk and fracture flow is that we obtain a rather effective scheme to describe the flow in the rock matrix while accounting for the presence of the fractures. Even if the analysis has been carried out so far for the problem with a single fracture we have shown with numerical experiments the capability of the scheme to deal with fracture networks.

Mimetic finite differences are indeed a natural choice to deal with this type of problems. The intersection of the fractures with an underlying grid for the matrix produces polygonal elements where we can apply the method directly, without the need of complex mesh generation algorithms to produce a standard grid conforming to the fractures. We wish to point out that, inspired from the model presented in [48], we have implemented rather general coupling conditions between the flow in the fractures and in the solid matrix. They may account for both "conductive fractures", *i.e.*, fractures with high permeability, and "sealing fractures", *i.e.*, fractures with low permeability which act as barrier to the flow. This differs from other works that adopt more simplified coupling conditions, which are justified only for very permeable fractures. Further on going developments include carrying out the full analysis of the problem with fracture networks and extending the implementation to three-dimensional problems. In this work, having carried out the numerical experiments only in 2D, we have solved the algebraic system with a direct multi-frontal scheme. Moving to the more challenging three-dimensional problems will require also to investigate suitable preconditioners to accelerate a Krylov-subspace iterative solver.

References

[1] P. Adler, J.-F. Thovert, and V. Mourzenko. *Fractured Porous Media*. Oxford University Press, 2013.

[2] O. Al-Hinai, S. Srinivasan, and M. F. Wheeler. Mimetic finite differences for flow in fractures from microseismic data. In *SPE Reservoir Simulation Symposium, 23-25 February, Houston, Texas, USA*. Society of Petroleum Engineers, 2015.

[3] C. Alboin, J. Jaffré, J. E. Roberts, X. Wang, and C. Serres. *Domain decomposition for some transmission problems in flow in porous media*, volume 552 of *Lecture Notes in Phys.*, pages 22–34. Springer, Berlin, 2000.

[4] P. Angot, F. Boyer, and F. Hubert. Asymptotic and numerical modelling of flows in fractured porous media. *M2AN Math. Model. Numer. Anal.*, 43(2):239–275, 2009.

[5] P. F. Antonietti, L. Beirão da Veiga, N. Bigoni, and M. Verani. Mimetic finite differences for nonlinear and control problems. *Math. Models Methods Appl. Sci.*, 24(8):1457–1493, 2014.

[6] P. F. Antonietti, L. Beirão da Veiga, C. Lovadina, and M. Verani. Hierarchical a posteriori error estimators for the mimetic discretization of elliptic problems. *SIAM J. Numer. Anal.*, 51(1):654–675, 2013.

[7] P. F. Antonietti, L. Beirão da Veiga, and M. Verani. A mimetic discretization of elliptic obstacle problems. *Math. Comp.*, 82(283):1379–1400, 2013.

[8] P. F. Antonietti, N. Bigoni, and M. Verani. Mimetic discretizations of elliptic control problems. *J. Sci. Comput.*, 56(1):14–27, 2013.

[9] P. F. Antonietti, N. Bigoni, and M. Verani. Mimetic finite difference approximation of quasilinear elliptic problems. *Calcolo*, 52(1):45–67, 2015.

[10] P. F. Antonietti, N. Bigoni, and M. Verani. Mimetic finite difference method for shape optimization problems. *Lecture Notes in Computational Science and Engineering*, 103:125–132, 2015.

[11] J. Bear, C.-F. Tsang, and G. de Marsily. *Flow and contaminant transport in fractured rock*. Academic Press, San Diego, 1993.

[12] L. Beirão da Veiga, F. Brezzi, A. Cangiani, G. Manzini, L. D. Marini, and A. Russo. Basic principles of virtual element methods. *Math. Models Methods Appl. Sci.*, 23(1):199–214, 2013.

[13] L. Beirão da Veiga, K. Lipnikov, and G. Manzini. Arbitrary-order nodal mimetic discretizations of elliptic problems on polygonal meshes. *SIAM Journal on Numerical Analysis*, 49(5):1737–1760, 2011.

[14] L. Beirao da Veiga, K. Lipnikov, and G. Manzini. *The Mimetic Finite Difference Method for Elliptic Problems*. Springer, 2014.

[15] L. Beirão da Veiga, C. Lovadina, and D. Mora. Numerical results for mimetic discretization of Reissner-Mindlin plate problems. *Calcolo*, 50(3):209–237, 2013.

[16] M. F. Benedetto, S. Berrone, S. Pieraccini, and S. Scialò. The virtual element method for discrete fracture network simulations. *Comput. Methods Appl. Mech. Engrg.*, 280:135–156, 2014.

[17] M. F. Benedetto, S. Berrone, and S. Scialò. A globally conforming method for solving flow in discrete fracture networks using the virtual element method. *Finite Elements in Analysis and Design*, 109:23– 36, 2016.
[18] M. Benzi, G. Golub, and J. Liesen. Numerical solution of saddle point problems. *Acta numerica*, 14(1):1–137, 2005.
[19] S. Berrone, S. Pieraccini, and S. Scialò. On simulations of discrete fracture network flows with an optimization-based extended finite element method. *SIAM J. Sci. Comput.*, 35(2):A908–A935, 2013.
[20] S. Berrone, S. Pieraccini, and S. Scialò. A PDE-constrained optimization formulation for discrete fracture network flows. *SIAM J. Sci. Comput.*, 35(2):B487–B510, 2013.
[21] S. Berrone, S. Pieraccini, and S. Scialò. An optimization approach for large scale simulations of discrete fracture network flows. *J. Comput. Phys.*, 256:838–853, 2014.
[22] S. Berrone, S. Pieraccini, S. Scialò, and F. Vicini. A parallel solver for large scale DFN flow simulations. *SIAM J. Sci. Comput.*, 37(3):C285–C306, 2015.
[23] K. Brenner, M. Groza, C. Guichard, G. Lebeau, and R. Masson. Gradient discretization of hybrid dimensional Darcy flows in fractured porous media. In J. Fuhrmann, M. Ohlberger, and C. Rohde, editors, *Finite Volumes for Complex Applications VII-Elliptic, Parabolic and Hyperbolic Problems*, pages 527–535. Springer, 2014.
[24] K. Brenner, M. Groza, C. Guichard, G. Lebeau, and R. Masson. Gradient discretization of hybrid dimensional Darcy flows in fractured porous media. Technical Report hal-01097704, HAL archives-ouvertes, December 2014.
[25] K. Brenner, J. Hennicker, R. Masson, and P. Samier. Gradient discretization of hybrid dimensional Darcy flows in fractured porous media with discontinuous pressures at the matrix fracture interfaces. In *MAMERN VI-2015*, 2015. HAL-01147495.
[26] F. Brezzi and A. Buffa. Innovative mimetic discretizations for electromagnetic problems. *J. Comput. Appl. Math.*, 234(6):1980–1987, 2010.
[27] F. Brezzi, A. Buffa, and K. Lipnikov. Mimetic finite differences for elliptic problems. *ESAIM: Mathematical Modelling and Numerical Analysis*, 43(02):277–295, 2009.
[28] F. Brezzi, A. Buffa, and G. Manzini. Mimetic scalar products of discrete differential forms. *J. Comput. Phys.*, 257(part B):1228–1259, 2014.
[29] F. Brezzi, K. Lipnikov, and M. Shashkov. Convergence of the mimetic finite difference method for diffusion problems on polyhedral meshes. *SIAM Journal on Numerical Analysis*, 43(5):1872–1896, 2005.
[30] F. Brezzi, K. Lipnikov, and M. Shashkov. Convergence of mimetic finite difference method for diffusion problems on polyhedral meshes with curved faces. *Math. Models Methods Appl. Sci.*, 16(2):275–297, 2006.
[31] F. Brezzi, K. Lipnikov, M. Shashkov, and V. Simoncini. A new discretization methodology for diffusion problems on generalized polyhedral meshes. *Comput. Methods Appl. Mech. Engrg.*, 196(37-40):3682–3692, 2007.
[32] F. Brezzi, K. Lipnikov, and V. Simoncini. A family of mimetic finite difference methods on polygonal and polyhedral meshes. *Mathematical Models and Methods in Applied Sciences*, 15(10):1533–1551, 2005.
[33] B. da Veiga Lourenco, K. Lipnikov, and G. Manzini. *The mimetic finite difference method for elliptic problems*, volume 11 of *MS&A. Modeling, Simulation and Applications*. Springer, Cham, 2014.
[34] C. D'Angelo and A. Scotti. A mixed finite element method for Darcy flow in fractured porous media with non-matching grids. *ESAIM: Mathematical Modelling and Numerical Analysis*, 46(02):465–489, 2012.
[35] J. Droniou. Finite volume schemes for diffusion equations: Introduction to and review of modern methods. *Mathematical Models and Methods in Applied Sciences*, 24(08):1575–1619, 2014.
[36] J. Droniou, R. Eymard, T. Gallouet, and R. Herbin. Gradient schemes: a generic framework for the discretisation of linear, nonlinear and nonlocal elliptic and parabolic equations. *Math. Models Methods Appl. Sci.*, 23(13):2395–2432, 2013.
[37] J. Droniou, R. Eymard, and R. Herbin. Gradient schemes: generic tools for the numerical analysis of diffusion equations. *Math. Model. Numer. Anal.*, to appear, 2015.
[38] G. Dziuk. Finite elements for the Beltrami operator on arbitrary surfaces. In *Partial differential equations and calculus of variations*, volume 1357 of *Lecture Notes in Math.*, pages 142–155. Springer, Berlin, 1988.
[39] R. Eymard, T. Gallouët, and R. Herbin. Finite volume methods. In P. Ciarlet and J.-L. Lions, editors, *Techniques of Scientific Computing, Part III, Handbook of Numerical Analysis, VII*, pages 713–1020. North Holland, 2000.
[40] A. Fumagalli and A. Scotti. A numerical method for two-phase flow in fractured porous media with non-matching grids. *Advances in Water Resources*, 62, Part C(0):454–464, 2013. Computational Methods in Geologic CO2 Sequestration.
[41] G. Guennebaud, B. Jacob, et al. Eigen v3. http://eigen.tuxfamily.org, 2010.
[42] H. Hægland, A. Assteerawatt, H. Dahle, G. Eigestad, and R. Helmig. Comparison of cell-and vertex-centered discretization methods for flow in a two-dimensional discrete-fracture–matrix system. *Advances in water resources*, 32(12):1740–1755, 2009.
[43] J. Jaffré, M. Mnejja, and J. E. Roberts. A discrete fracture model for two-phase flow with matrix-fracture interaction. *Procedia Computer Science*, 4:967–973, 2011.
[44] M. Karimi-Fard, L. Durlofsky, K. Aziz, et al. An efficient discrete-fracture model applicable for general-purpose reservoir simulators. *SPE Journal*, 9(02):227–236, 2004.
[45] K. Lipnikov, G. Manzini, and M. Shashkov. Mimetic finite difference method. *Journal of Computational Physics*, 257, Part B(0):1163 – 1227, 2014. Physics-compatible numerical methods.
[46] K. Lipnikov, J. D. Moulton, and D. Svyatskiy. A multilevel multiscale mimetic (M^3) method for two-phase flows in porous media. *J. Comput. Phys.*, 227(14):6727–6753, 2008.

[47] B. Mallison, M. Hui, and W. Narr. Practical gridding algorithms for discrete fracture modeling workflows. In *12th European Conference on the Mathematics of Oil Recovery*, 2010.
[48] V. Martin, J. Jaffré, and J. E. Roberts. Modeling fractures and barriers as interfaces for flow in porous media. *SIAM Journal on Scientific Computing*, 26(5):1667–1691, 2005.
[49] H. Mustapha. A Gabriel-Delaunay triangulation of 2D complex fractured media for multiphase flow simulations. *Computational Geosciences*, 18(6):989–1008, 2014.
[50] J. E. Roberts and J.-M. Thomas. Mixed and hybrid methods. In *Handbook of numerical analysis. Finite Element Methods (Part I)*, volume 2, pages 523–639. Elsevier, 1991.
[51] The CGAL Project. *CGAL User and Reference Manual*. CGAL Editorial Board, 4.6 edition, 2015.